Simulation studies on creation and propagation of UHE-photons with CRPropa

Biswajit Sarkar

Diplomarbeit

Fachbereich Physik
Bergische Universität Wuppertal

Contents

Contents

1 Introduction

Nearly one century ago Victor Hess discovered the existent of cosmic rays (CR) that hit Earth every day from outside the atmosphere. This discovery had fundamental impact on particle physics. Until today many questions related to sources of this particles and their propagation from their origin to us are not answered. For example a big problem is posed by Galactic and intergalactic magnetic fields, which make the charged cosmic rays forget their original direction. One of the most promising candidate which might keep the information of their sources are cosmic rays on the upper end of the measured energy scale, as these particles should suffer less deflections in magnetic fields. In addition other components, which are not or even less effected by magnetic field, like very high energetic neutrinos or photons might provide us with additional clues.

Hence, the aim of this thesis is to provide prediction on the expected flux and directional information of ultrahigh energetic (energy $> 10^{18}$ eV, UHE) photons that should be produced during the propagation of ultrahigh energetic nucleons or in the sources themselves. In this thesis simulation studies with the Monte Carlo code CRPopa[1] are performed. This numerical tool offers the possibility to simulate the intergalactic propagation of nucleons and their secondaries like photons.

2 Cosmic Rays

2.1 Energy spectrum

Cosmic rays are measured in a huge energy range, that extends over twelve orders of magnitude from a few hundred MeV to 300 EeV, in which the flux per energy decreases nearly thirty-one orders of magnitude as one can see in figure 2.1(a). So starting from more than 1000 particles per second and square meter for cosmic ray energies of a few GeV only less than one particle per km^2 and century are measured above 100 EeV. Because of this, the necessary detection area to collect enough statistics in a reasonable time period have to grow for higher particle energies. Up to 10^{15} eV direct measurements above the atmosphere are realised till now. For higher energies only ground based experiments exists. The energy spectrum follows approx-
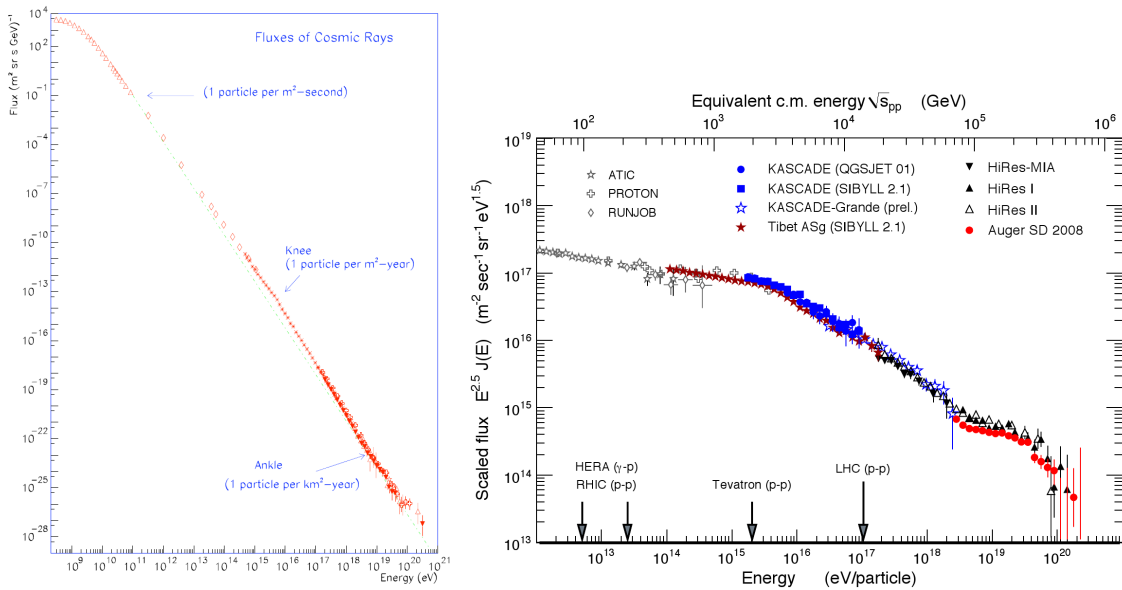
(a) All-particle cosmic-ray energy spectrum [2]

(b) All-particle cosmic-ray energy spectrum multiplied with $E^{2.5}$ [3]

Figure 2.1: All-particle cosmic-ray energy spectrum

imately a powerlaw in energy

$$dN/dE \propto E^{\alpha},$$

which shows a few structures at different energies, which can be seen in figure 2.1(b), where the flux is multiplied with $E^{2.5}$ to amplify the changes in the shape. Up to energies of $4 \cdot 10^{15}$ eV the spectral index is $\alpha \approx -2.7$. After this so called knee position the spectrum becomes steeper with $\alpha \approx -3.1$. This is explained by a reduction of the flux of lighter particles. At $10^{17.5}$ eV a second knee is positioned, whose validity is still disputed. Above $10^{18.5}$ eV the spectrum is flattened again to a spectral index of $\alpha \approx -2.69$. This is usually explained by the transition from galactic to extragalactic origin of the cosmic ray particle. And finally, from $4 \cdot 10^{19}$ eV on a stronger steepening is observed, which matches to a spectral index of $\alpha \approx -4.2$. Theories for this bending are discussed in section 2.3.

2.2 Chemical composition of cosmic rays

In fact all elements of the periodic table are found in cosmic rays. Below the energy of 10^{14} eV the spectra of the individual elements can be directly measured above the atmosphere by experiments on satellites or balloons. The relative abundances of the elements in cosmic rays measured by different experiments at an energy of 1 GeV/n are shown in figure 2.2(a) in comparison to the relative abundances of elements in the solar system. In general there is a good agreement between these two distributions, except to an excess in the light elements like lithium, beryllium, boron as well as elements just below iron or lead in cosmic rays. Assuming that the cosmic rays have at there origin the same composition like the elements in the solar system, the described overabundances could be the result of spallation processes of the CNO, iron and lead groups with interstellar dust and gas particles during their propagation through the Galaxy.

Above 10^{15} eV only ground based observations are possible, which use air showers initiated by cosmic rays in the atmosphere to conclude on the primary cosmic ray particle. Here the ratio of electron and muon numbers at ground level or the depth of the shower maximum are used to distinguish between the different mass groups. Because the atmosphere has not a constant density, the depth of the shower maximum is measured in atmospheric slant depth X, which is measured in [g/cm^2], which measures the length in equidistant intercepts of traversed matter density instead of meters. The maximum (X_{max}) of showers induced by heavier elements should be higher up in the atmosphere than for lighter elements. The results of the X_{max} measurements from different experiments are shown in figure 2.2(b). Below the knee energy (see section 2.1), which is $4 \cdot 10^{15}$ eV, the average composition seems to become lighter, whereas above this value the average mass decreases until $4 \cdot 10^{16}$ eV. For higher energies again a shift to lighter composition is indicated. New data from the Pierre Auger Observatory indicates a break towards heavier elements at energies at about $2 \cdot 10^{18}$ eV.
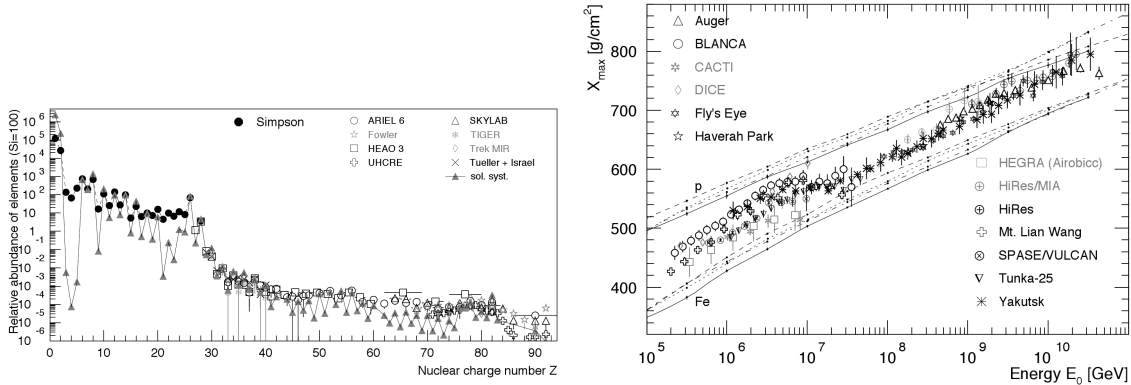
(a) Abundances of of the different elements in the cosmic rays of 1 Gev/n.[3]

(b) Average depth of the shower maximum Xmax as function of primary energy as measured by different experiments.[3]

Figure 2.2:

2.3 GZK-effect

In 1966 Greisen[4] and independently Zatsepin and Kuzmin[5] concluded, that nucleons with energies above $5 \cdot 10^{19}$ eV should lose energy on their way from their sources to earth, by producing pions in interactions with low energetic background photons, which are Lorentz transformed in the rest frame of the nucleon. The cross section for this photo-pion production increases strongly at the $\Delta^+(1232)$ resonance. In case of a proton, the process can be described as

$$
\begin{aligned}
p + \gamma_b \rightarrow \Delta^+(1232) &\rightarrow p + \pi^0 \\
&\rightarrow n + \pi^+.
\end{aligned}
$$
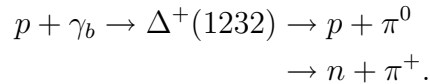
For higher energies also further baryonic resonances like $\Delta(1620)$ and $\Delta(1700)$ and further processes like

$$
p + \gamma_b \rightarrow \Delta^{++} + \pi^- \rightarrow p + \pi^+ + \pi^-
$$
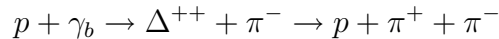
become possible. The most important photon background for the photo-pion production is the cosmic microwave background, but also the the infrared background plays a significant role for nucleon energies between 10^{17} eV and $5 \cdot 10^{19}$ eV.

The consequence of this effect, which is called the GZK-effect, would be the steepening of the cosmic ray spectrum at energies above $5 \cdot 10^{19}$ eV, which is then called GZK-suppression. As described in section 2.1, such a behaviour is seen in the measurements of the HiRes experiment [6] and The Pierre Auger Observatory [7]. But this is not a clear proof of the GZK-suppression, because also other explanations of

7

the observed steepening exists like the exhaustion of the acceleration processes. A support for the existents of the GZK-suppression is provided by the correlation of the arrival direction of the cosmic rays with AGN, which is seen by the Pierre Auger Observatory. This indicates an anisotropy of the arrival direction distribution, that appears for energies above 57 EeV [8].

2.4 UHE Photon

Until now only photon energies up to 10^{14} eV are observed. But many theoretical models for ultra high energetic cosmic ray production or propagation predict also a photon component with these energies, whose observation would open a new window in cosmic-ray research. In most models UHE-photons are produced by the decay of neutral pions, which are produced either in the decay or annihilation of primordial relics such as topological defects (TD) or super heavy dark matter particles (SHDM) or by the GZK-effect during the propagation of UHE-nuclei, as described in chapter 2.3. Another possible source would be the Z-burst scenario, where the photon would be generated in the decay of a Z-boson, which is produced in scattering of UHE-neutrinos on cosmological relic neutrinos.
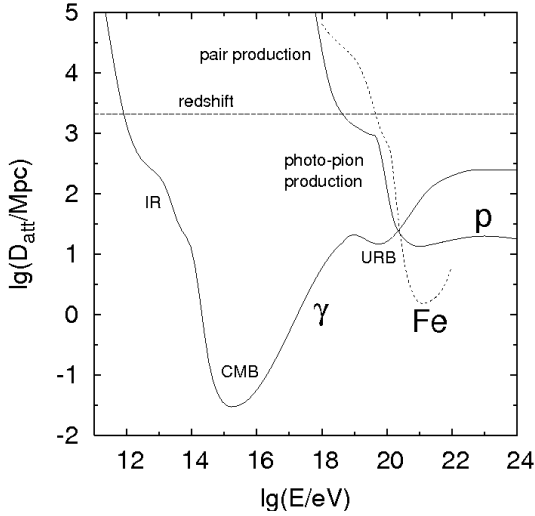
(a) Energy loss length [9]
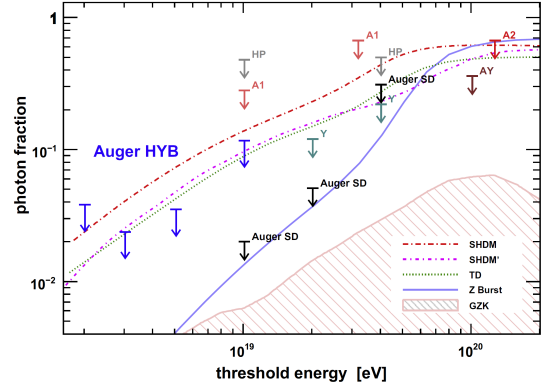
(b) Upper limits on the photon fraction in the integral cosmic ray flux from different experiments: AGASA(A1,A2), AGASA-Yakutsk(AY), Yakutsk(Y), Haverah Park(HP) [10]

Once produced these UHE-photons can generate electromagnetic cascades by interacting with the low energy photon background(γ_b). The relevant interaction for

this cascades are

pair production	$\gamma + \gamma_b$	$\rightarrow$	$e^+ + e^-$
double pair production	$\gamma + \gamma_b$	$\rightarrow$	$e^+ + e^- + e^+ + e^-$
inverse Compton scattering	$e + \gamma_b$	$\rightarrow$	$e + \gamma$
triplet pair production	$e + \gamma_b$	$\rightarrow$	$e + e^+ + e^-$

High energetic photons produce multiple electrons and positrons, which again produce high energetic photons by inverse Compton scattering. This new photons again produce high energetic electrons and positrons and the cascade goes continues. In these electromagnetic cascades, the photons lose energy until their energy falls in the GeV to TeV region, where the universe becomes transparent for photons, as can be seen in figure 2.3(a).

Although no photons are seen in current observations, experiments were able to place upper limits to the fraction of these photons in the cosmic ray flux as shown in figure 2.3(b). The most stringent limits at present are set by the Pierre Auger Observatory. They are listed in table 2.1.

Threshold energy	Upper limit (95 % c.l.) for photon fraction
$2 \cdot 10^{18}$ eV	3.8%
$3 \cdot 10^{18}$ eV	2.4%
$5 \cdot 10^{18}$ eV	3.5%
$10 \cdot 10^{18}$ eV	2%
$20 \cdot 10^{18}$ eV	5.1%
$40 \cdot 10^{18}$ eV	31%

Table 2.1: Upper limits (at 95 % c.l.) for the photon fraction set by the Pierre Auger Observatory [11] [10]

3 Extragalactic magnetic fields

Observations show magnetic fields of different strength in the Universe in huge structures like galaxies ($\sim 1\mu G$ - $\sim 10\mu G$) [12], in galaxy clusters (a few μG) [13] and even filament of superclusters [14].

Theoretical models exist, which explain these fields as a combination of two processes. At first a primary seed field is needed. Candidates for these seeds are primordial magnetic fields produced for example during the electroweak phase transition right after the big bang or fields produced through cluster acceleration shocks in the so called Biermann battery effect [15]. Once such a seed exists it can be amplified through magnetohydrodynamical processes during the large scale structure formation processes of the Universe in which galaxies, galaxy clusters and superclusters were formed. This could for example explain the fields measured in galaxy clusters.

For the propagation of cosmic rays especially the spaces between superclusters, the so called voids, are importend. As magnetic field measurements of this regions were not successfull till now, simulations based on the mentioned theories are made predict the magnetic fields in this regions.

In section 6.4 a magnetic field map from such a simulation made by Miniati et al. [16] will be used. Here the mentioned large scale structure formation processes and the effect they have on magnetic seed fields, which are set at the beginning, are simulated. For the map used here, seed fields resulted from the Biermann battery effect are assumed. The initial distribution of these seeds are chosen arbitrarily so that the localisation of the magnetic field structure in the end have no correlation with the real Universe. But the strength and structure should be realistic. The simulation predict magnetic fields in the voids of the order of $10\,\mathrm{fG}$ and an average field in the whole simulated space of the order of $10\,\mathrm{nG}$ [17].

4 CRPropa

As described before, the energy spectra and arrival directions of ultra high energy cosmic rays observed at Earth, are strongly influenced by effects happening on their way from possible sources to us. For a better understanding of these effects it is necessary to perform computer simulations of these processes. CRPropa is a publicly-available numerical tool that was created by Eric Armengaud et al. [1] for this purpose. It is capable of propagating nucleons and secondary electromagnetic cascades (em cascades) and neutrinos, produced during the nucleon propagation. In fact, CRPropa is a combination of two tools. The fist one is a Monte Carlo code for simulating tree-dimensional propagation in a magnetized Universe and taking in account energy losses due to interactions with the low energy background photons (mainly CMB). The second part is a 1-dimensional transport code that solves em-cascades and neutrino propagation.

The two interactions of nucleons during their propagation, which are considered so far in CRPropa are photo-pion production and pair production, both with the low energy photon background. The SOPHIA event generator, which employs particle production cross sections measured in particle accelerators, is used to handle the pion production. In each timestep of the simulation it decides whether an interaction takes place for each trajectory. If this is the case, SOPHIA determines the energy and type of the stable particles generated in the whole interaction. Pair production by protons on the CMB is treated as a continoues energy loss for the protons using tables derived from the DINT [18]package. The energy distribution of the produced electron-positron-pairs is approximated with $dN/dE \propto E_e^{-7/4}$.

The tracking of secondaries, namely electrons, positrons, photons and neutrinos is possible. Neutrinos propagate in straight lines without any energy loss except those due to redshift. The other three particles interact on their way with the low energy photon background and therefore evolve trough an electromagnetic cascade, which is calculated again using tables derived from the DINT package. Here all relevant interactions are taken in account. These are pair production, double pair production, triplet pair production and inverse Compton effect. In the presence of extragalactic magnetic fields also synchrotron losses of electrons and positrons are included and the EM-cascades resulting from the synchrotron-photons are also followed. Because of the deflections of the charged components of the EM-cascade in the magnetic fields the 1-dimensional treatment of them is only an approximation. But as shown in [20] the deflection can be neglected.
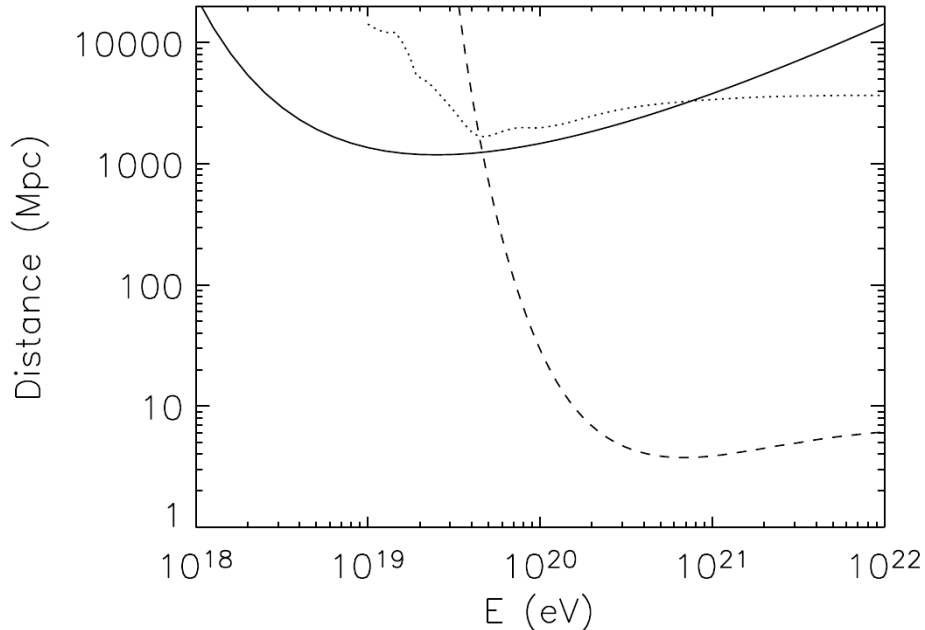
Figure 4.1: Proton energy loss length by pair production in the CMB (continuous line), interaction length for pion production in the CMB (dashed line) and Primack et al. [19] IRB (dotted line) at z=0.

The most important low energy photon background for the here regarded interactions is CMB. But also infrared background (IRB) and the universal radio background (URB) influence the cosmic ray propagation. Because the density distribution of these two backgrounds are not exactly known, there are three versions of each of them implemented in CRPropa. For the IRB a low and a high version of Franceschini et al. [21] and one by Primack et al. [19] are implemented. In the case of the URB the alternatives are a weak and a strong version calculated by Protheroe et al. [22] and one distribution based on observations by Cleark et al. [23].

The simulation can be run in two different modes. In 1d-mode all particles only follow a straight path from the source to the observer. Obviously no deflections in magnetic field are possible. Red-shift losses can be taken into account in this mode. In the three dimensional case particles propagate in a "simulation box" with periodic boundary conditions. That means that whenever a particle reaches a boundary surface of the simulation box it reenters in the opposite surface. In this mode different magnetic fields can be implemented inside the box which are then used to calculate the deflections. But as the distance, the proton have to travel to arrive at the observer, is not known at the beginning of each simulation, redshift losses can not be taken into account in the three dimensional mode.

Cosmic rays in CRPropa can originat continuously in a region of space as well as

from point sources. The energy can be set to a discrete value or follow a power law distribution.

Two different storing modes are provided where in "full trajectories" coordinates and other properties of the nucleons are stored in every timestep and in "events" only the data for particles arriving at an observer is saved. Secondaries are only available in the events case. In case of the em cascade the full energy spectrum from 10^{24} eV down to 10^7 eV is stored. Here for each logarithmic energy bin the mean number of particles is stored. This number can also be smaller than one.

5 Studies with a one dimensional propagation model

5.1 Aim

In this first part, the UHE γ flux, arriving from single point sources emitting ultra high energetic particles with only discrete energies, is analysed with the one dimensional model. The aim here is to study the dependence of the integral photon flux above different energy thresholds on the energy (E_S) of the particles at the source and the distance (D) of the source from the observer for different scenarios. For this reason these two parameters are varied in the ranges between $10^{18} - 10^{24}$ eV and $1 - 200$ Mpc respectively, in a series of simulations. The values for the detection thresholds are $E_{\text{thr}} = 10^{17}$ eV, $E_{\text{thr}} = 10^{18}$ eV and $E_{\text{thr}} = 10^{19}$ eV. For each of these threshold energies the result will be an energy-distance matrix which shows the wanted dependences.

5.2 Photon sources

In the beginning sources are assumed which emit only photons. This is mainly for the understanding of the electromagnetic cascades (em-cascades) induced by UHE-photons, but is also one possible source scenario, as described in section 2.4. As the propagation of the em-cascades is an analytic calculation, no fluctuation is expected and only one photon have to be started for each simulation. The starting energies for the photons are increased in 0.1 steps in the logarithmic scale of the energy.

5.2.1 Expected behaviour

From the properties of the electromagnetic cascades, one can predict how the number of photons at the observer should qualitatively behave with the variation of the source distance and the source energy. As described in section 2.4, the cascading increases the number of photons for the here regarded energies. Along with the increase of the photon number obviously the energy of the photons decreases. Since only photons above a threshold energy are observed, the cascading increases the number of these photons only up to the point, where the produced photons start to drop below the threshold energy. For photon energies above the threshold, consequently an increase

in the number is expected for small source distances and a decrease in number for larger distances. Between this two regions a distance should exist, where a maximum number of photons above a threshold reach the observer. This distance should move to smaller values for lower source energies.

(a) $E_{\mathrm{thr}}=10^{18}$ eV

(b) $E_{\mathrm{thr}}=10^{17}$ eV
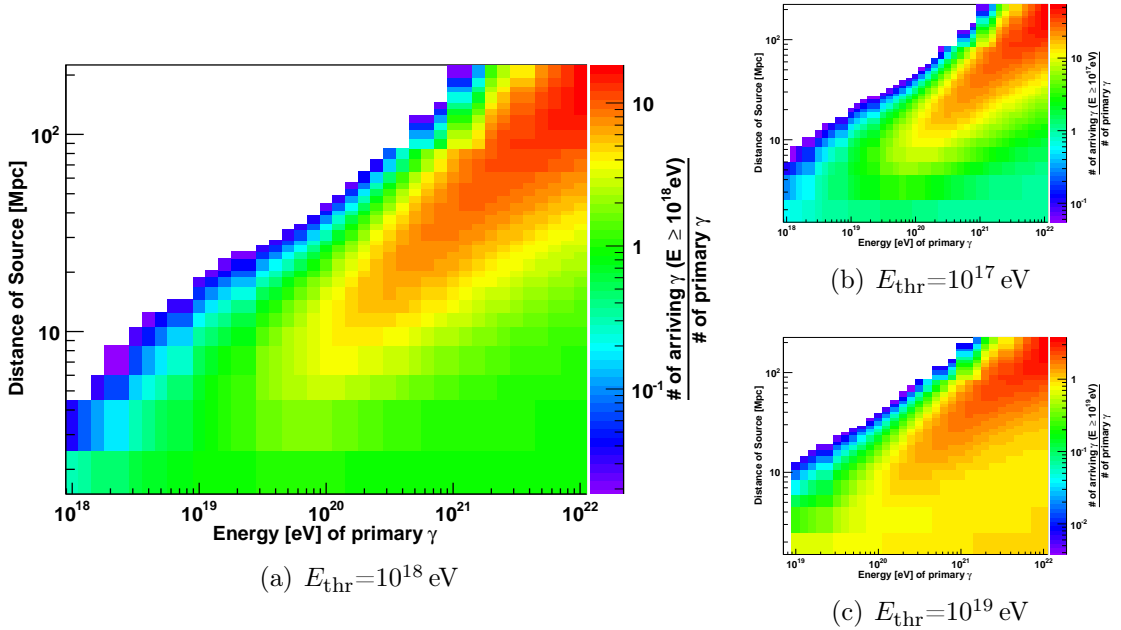
(c) $E_{\mathrm{thr}}=10^{19}$ eV

Figure 5.1: Energy-distance matrix for primary photons for different energy thresholds

5.2.2 Results

The resulting energy-distance matrices for the photon number above threshold energies of $E_{\mathrm{thr}} = 10^{17}$ eV, $E_{\mathrm{thr}} = 10^{18}$ eV and $E_{\mathrm{thr}} = 10^{19}$ eV at the observer, heretoafter abbreviated by N_γ^{obs}, per source photon is shown in the figure 5.1. For each of this threshold energies the development of the photon number with increasing D is different for two E_{S} regions. For higher E_{S} at first the N_γ^{obs} increases until a maximum is reached and then a continuous decrease begins, which is exactly in agreement with the expectations. For lower E_{S} just a decrease with distance is observed. This indicates that already the photons emitted from the source produce in the electromagnetic cascades in average only photons below the given threshold energy. The source energies, above which the first behaviour sets in, are $E_{\mathrm{S}} = 10^{18.5}$ eV, $E_{\mathrm{S}} = 10^{19.1}$ eV and $E_{\mathrm{S}} = 10^{20}$ eV for the threshold energies of $E_{\mathrm{thr}} = 10^{17}$ eV, $E_{\mathrm{thr}} = 10^{18}$ eV and $E_{\mathrm{thr}} = 10^{19}$ eV, respectively.

Especially interesting is the distance of the photon emitting source, of which the maximum number of photons above a given detection threshold is expected to reach

(a) $E_{\text{thr}}=10^{18}$ eV   (b) $E_{\text{thr}}=10^{17}$ eV   (c) $E_{\text{thr}}=10^{19}$ eV
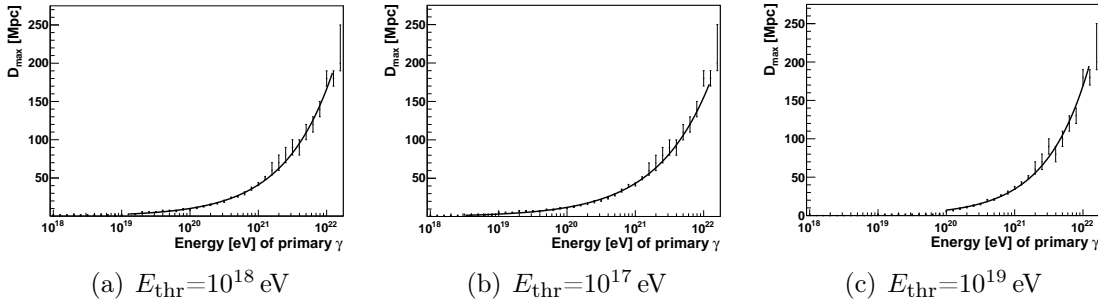
Figure 5.2: The points show the D_{max} in dependence on E_{S} . The black line shows the fit to this values.

the observer. For each source energy this distance, heretoafter called distance of maximum (D_{max}), and the number of photons in this maximum ($_{\text{max}}N_\gamma^{\text{obs}}$) is estimated. As a very clear maximum exists for the region of higher source energies, it is sufficient just to take that distance and the photon number in the according simulation. The results are shown in figure 5.2 and 5.3. The upper and lower uncertainties of D_{max} are estimated by taking the gap to the next higher and lower distances, that are simulated in the energy distance matrix. For the $_{\text{max}}N_\gamma^{\text{obs}}$ values the uncertainties for the photon number are estimated as zero, because the number of photons are just calculated by a DINT parameterisation. To quantify the energy dependence of these two values, a parameterisation is given for both of them, each for all three energy thresholds. The here derived formulas are not physically motivated. Their aim is rather to find a way to describe the found behaviour with a low number of parameters. These parameterisations could be useful to estimate, whether a large flux of UHE photons can be expected for some source distribution scenarios. To derive the parameters the method of least squares [24] is used for all parameterisations in this chapter.

The ansatz for the maximum distance is

$$D_{max}(E_S) = p_0 \cdot (E_S)^{p_1}. \tag{5.1}$$

Applying this ansatz to the D_{max} values derived from the simulation matrices determines the parameters p_0 and p_1 for each threshold, which are listed in table 5.1.

E_{thr}[eV]	p_0	p_1	Valid for E_{S} [eV] above
10^{17}	$1.028 \cdot 10^{-10}$	0.5536	$10^{18.5}$
10^{18}	$7.254 \cdot 10^{-12}$	0.6073	$10^{19.1}$
10^{19}	$1.137 \cdot 10^{-13}$	0.6896	10^{20}

Table 5.1: Parameters derived by fitting D_{max}

(a) $E_{\mathrm{thr}}=10^{18}$ eV   (b) $E_{\mathrm{thr}}=10^{17}$ eV   (c) $E_{\mathrm{thr}}=10^{19}$ eV
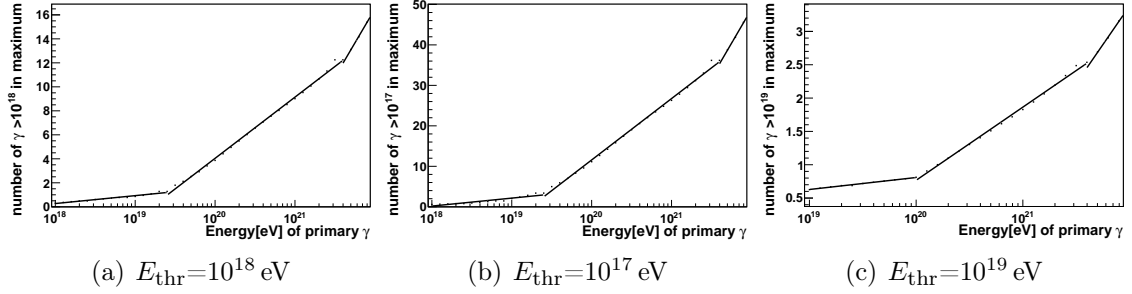
Figure 5.3: The points show $_{\max}N_\gamma^{\mathrm{obs}}$ in dependence on E_{S} . The black line shows the fit to this values.

The number of photons above a threshold observed in the maximum is described in three subranges: $R_1 : 10^{18} - 10^{19.4}$ eV, $R_2 : 10^{19.4} - 10^{21.6}$ eV and $R_3 10^{21.6} - 10^{22.3}$ eV. In each range the ansatz

$$_{\max}N_\gamma^{\mathrm{obs}}(E_S) = p_0 \cdot log_{10}(E_S) + p_1 \tag{5.2}$$

is made. The parameters p_0 and p_1 determined for $_{\max}N_\gamma^{\mathrm{obs}}(E_S)$ are listed in table 5.2.

E_{thr}[eV]	Energy range	p_1	p_0
10^{17}	R_1	-35.23	1.967
	R_2	-291.7	15.17
	R_3	-694.8	33.8
10^{18}	R_1	-11.59	0.6589
	R_2	-98	5.102
	R_3	-232.5	11.32
10^{19}	R_1	-2.785	0.1797
	R_2	-21.18	1.097
	R_3	-47.66	2.32

Table 5.2: Parameter derived by fitting $_{\max}N_\gamma^{\mathrm{obs}}$

5.3 Proton sources

In the previous section the behaviour of the electromagnetic cascades was discussed in detail. The focus of this section is the photon component of UHE cosmic rays produced during the propagation of nucleons. In this simulation, protons are emitted from the source instead of photons as in section 5.2. This is a more realistic source scenario. The ranges for the source energy and the source distance are the same as in the previous simulation.

5.3.1 Preparations

Estimating the stepsize of the algorithm of the simulation

To estimate the best value for the timesteps of the simulation, one has to find a good compromise between accuracy of the simulation, which increases with smaller steps, and CPU time, which increases with bigger steps. For the accuracy it is reasonable to choose the time steps somewhat smaller than the smallest interaction length for protons in the regarded energy range $10^{17}-10^{24}$ eV, which is bigger than 3 Mpc as one can see in figure 4.1. In addition, one has to take care that in CRPropa the probability of one nucleon to undergo an interaction $P = 1 - e^{D/\lambda}$ is calculated by using the first order Taylor series of this expression D/λ. Where λ is the interaction length. The accuracy of this expression also rises with smaller time steps. To make an estimation for this behaviour, simulations with different stepsizes, where all other parameters are fixed, are performed. As a degree of accuracy the value for the interaction length of the protons, emitted at the source, is calculated from the output of this simulations. To do this, the number (N) of protons, which have still their starting energy, are assumed to be those from the $N_{\mathrm{p}}^{\mathrm{src}}$ protons emitted at the source, that have not undergone any interaction within the propagation distance D. The interaction length can then be expressed as $\lambda = -D(\ln(\frac{N(D)}{N_{\mathrm{p}}^{\mathrm{src}}}))^{-1}$. With a source energy of 10^{21} eV and a source distance of 2 Mpc one obtains the results shown in table 5.3. Comparing these values to the value $\lambda_{lit} = 3.6$ Mpc derived from figure 1. from [25] shows a good approach for a stepsize of 0.01 Mpc.

Size of timestep [Mpc]	λ [Mpc]
1	6.64
0.06	3.79
0.01	3.67

Table 5.3: Estimation of interaction length.

To estimate the increase in CPU time due to the smaller stepsizes again simulations are run with different stepsizes for a source distance of 11 Mpc and a starting statistics

of 50000 protons shown in table 5.4.

Size of timestep [Mpc]	CPU time [sec]
1	240
0.1	330
0.05	430
0.01	1290

Table 5.4: Estimation of CPU time.

From these two rough estimations a stepsize of $0.05\,\mathrm{Mpc}$ is taken as the best compromise and therefore used in the following simulation.

Recent more detailed studies of accuracy of the simulations, show that a stepsize of $0.1\,\mathrm{Mpc}$ would be also sufficient.

Estimating the right amount of statistics for the simulation

The next question that arises is how much statistics is needed in each simulation to keep the relative fluctuation of the value of interest, here N_γ^{obs} divided by the number of source protons, under a reasonable limit. To answer this question for one point in the energy distance matrix a simulation is repeated forty times with different random seeds. Calculating the ratio of the root mean square(RMS) and the mean of the distribution from $\frac{N_\gamma^{\mathrm{obs}}}{N_p}$ from these forty simulations, gives then a degree of the relative fluctuation. This is done for different amounts of statistic, meaning different numbers of protons emitted from the source, to estimate the statistics needed for determining the fluctuations to a level of better than one percent.

Because doing this analyses for all combinations of source energy and distances would cost far too much computation time, one can only do this for a few chosen points. Therefore, the whole energy distance matrix is simulated once with 50000 primary protons in each simulation. This shows already, that the interesting feature of the maximum distance, like in the previous section, also appears here. As the aim is again to study this maximum, the fluctuations should be small in this region. Therefore, a distance of 14 Mpc is taken, which is close to the maximum for energies up to $10^{21}\,\mathrm{eV}$, as one can see in figure 5.6. The resulting relative fluctuations are shown in table 5.5.

Demanding a very conservative limit for the fluctuations of 0.005, a statistics of 50000, 500000 and 5000000 primary protons is used for the source energies ranges of $10^{21.1} - 10^{24}\,\mathrm{eV}$, $10^{19.9} - 10^{21}\,\mathrm{eV}$ and $10^{19.4} - 10^{19.8}\,\mathrm{eV}$ respectively. For lower energies $\frac{N_\gamma^{\mathrm{obs}}}{N_p}$ is neglectable small and because of this not regarded any more.

Source energy [eV]	$\frac{\text{RMS}}{\text{Mean}}$ for 50000 source protons	$\frac{\text{RMS}}{\text{Mean}}$ for 500000 source protons	$\frac{\text{RMS}}{\text{Mean}}$ for 5000000 source protons
10^{22}	0.004	0.001	
10^{21}	0.002	0.001	
10^{20}	0.007	0.002	
$10^{19.9}$	0.01	0.004	
$10^{19.8}$	0.017	0.006	0.002
$10^{19.6}$	0.022	0.007	0.002
$10^{19.4}$	0.027	0.010	0.003

Table 5.5: Relative fluctuations of the number of observed photons above an energy of $E_\gamma > 18$ eV per primary proton for different source energies and number of source protons.

5.3.2 Expected behaviour

For this simulation series, the integral flux of photons above threshold energies of $E_{\text{thr}} = 10^{17}$ eV, $E_{\text{thr}} = 10^{18}$ eV and $E_{\text{thr}} = 10^{19}$ eV should be caused by a combination of two effects. Since only protons are emitted at the source, photons have to be created during the propagation by photo-pion production and proton pair production, as described in chapter 4. These processes go on and increase the photon number until the nucleon energy drops under $\sim 5 \cdot 10^{19}$ eV, where the dominant first production process stops. The second effect is the electromagnetic cascading the photons undergo, once they are produced. The effect on the photon number is discussed in section 5.2. It causes an increase in the photon number as long as the energies of the particles in the cascade are high enough to produce photons above the threshold. But after longer propagation, the cascading should lead always to a decreasing number of photons. The final photon number at the observer is the result of the combination of these effects. For short source distances the two photon production processes should be dominant and therefore an increase in photon number should be observed. But with increasing distance more protons should reach the energies, where they undergo less interactions and therefor produce less photons. Hence, again a source distance should exist for each threshold, where a maximum number of photons above the threshold energy should be observed. For higher source distances, more photons should drop under the threshold energy through the cascading process than are produced due the cascading and the proton propagation. This should decrease the number of observed photons.

(a) $E_{\text{thr}} = 10^{18}$ eV

(b) $E_{\text{thr}} = 10^{17}$ eV

(c) $E_{\text{thr}} = 10^{19}$ eV
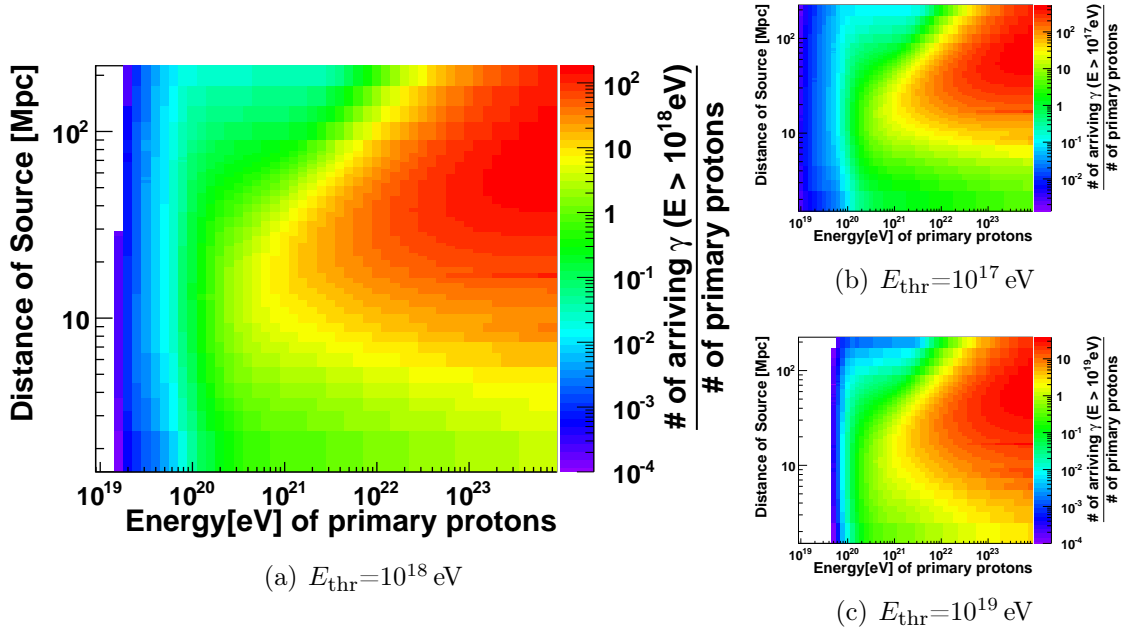
Figure 5.4: Energy-distance-matrix for primary protons and different thresholds applied to the observed photon energy

5.3.3 Results

The N_γ^{obs} values per primary proton are shown in figure 5.4. The distance behaviour for fixed source energies is qualitative the same for all source energies. It is similar to the behaviour, that could be observed in the last section for higher source energies. The fraction $\frac{N_\gamma^{\text{obs}}}{N_{\text{p}}^{\text{src}}}$ is monotonically increasing with the distance until one maximum is achieved, after which a continuous decrease starts. This is in exact agreement with the expectations. For source energies up to $10^{19.8}$ eV only a very slow decrease with distance is observed, compared to higher source energies. This can be seen in figure 5.5, which shows slices through the energy distance matrix for fixed source energies. Although also a maximum can be seen here, for these energies one can speak of nearly constant flux of UHE photons expected for sources up to 100 Mpc. The reason for this behaviour is that for this nucleon energies the pair production process is the dominant interaction that produced the cascades. As the energy loss length for this process is very large (in the order of 10^3 Mpc) and the threshold under which it stops lower than in the case of the pion production, the nucleons continue producing photons in the regarded distance range.

The energy dependence of the maximum distance and the $_{\text{max}}N_\gamma^{\text{obs}}$ value are described in the figures 5.6 and 5.7. In the case of the maximum distance one single

(a) $E_{\mathrm{S}} = 10^{19.8}$ eV

(b) $E_{\mathrm{S}} = 10^{21}$ eV
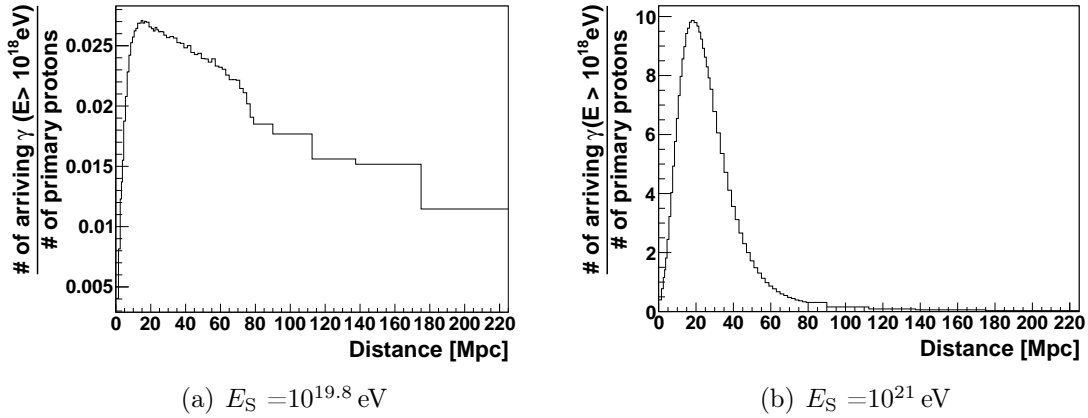
Figure 5.5: Cross section through the energy distance matrix for fix source energies

parameterization for the whole range of source energies can not be found, without using to many parameters. Because of this it was decided to split the whole source energy range into the two subranges $R_1 : 10^{19.4}\, eV \leq E_S \leq 10^{20.5}$ eV and $R_2 : 10^{20.5}\, eV \leq E_S \leq 10^{24}$ eV. The uncertainties are estimated as for $D_{\max}$ in case of photon sources. The according ansatz for the parameterization is:

$$
D_{\max}(E_{\mathrm{S}}) =
\begin{cases}
p_3 \cdot (\log_{10}(E_{\mathrm{S}}))^3 + p_2 \cdot (\log_{10}(E_{\mathrm{S}}))^2 + p_1 \cdot \log_{10}(E_{\mathrm{S}}) + p_0 & E_{\mathrm{S}} \in R_1, \\[2ex]
p_2 \cdot (\log_{10}(E_{\mathrm{S}}))^2 + p_1 \cdot \log_{10}(E_{\mathrm{S}}) + p_0 & E_{\mathrm{S}} \in R_2.
\end{cases}
$$

(5.3)

Fitting this functions to the points derived from the simulation series defines the set of parameters for each photon energy threshold, which are summarized in the table 5.6.

E_{thr}[eV]	Energy range	p_3	p_2	p_1	p_0
10^{17}	R_1	27.91	-1682	$3.377 \cdot 10^4$	$-2.26 \cdot 105$
	R_2		1.949	-69.86	627.5
10^{18}	R_1	31.04	-1871	$3.758 \cdot 10^4$	$-2.516 \cdot 10^5$
	R_2		1.814	-64.1	564.4
10^{19}	R_1	0.2217	-4.493	-90.42	1841
	R_2		1.651	-57.63	496.8

Table 5.6: Parameters derived by fitting the ansatz to the simulated data

(a) $E_{\text{thr}}=10^{18}$ eV   (b) $E_{\text{thr}}=10^{17}$ eV   (c) $E_{\text{thr}}=10^{19}$ eV
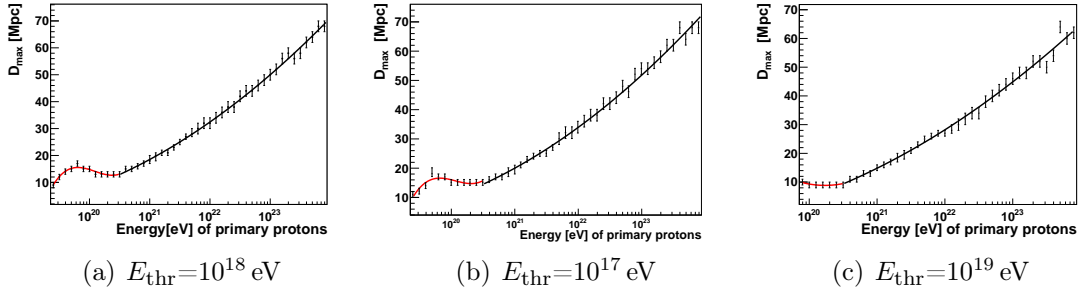
Figure 5.6: The points show D_{max} in dependence of E_{S} for the simulation series with primary protons. The black and the red line shows the parameterization of these values.

For the E_{S} dependence of the $_{\text{max}}N_\gamma^{\text{obs}}$ values from this simulations no ansatz is found, that gives a good χ^2 from the method of least squares. One reason for this could be the very small uncertainties, which is estimated from $\sqrt{_{\text{max}}N_\gamma^{\text{obs}}}$. An ansatz that fits the points, as one can see by eye in figure 5.7 is

$$_{\text{max}}N_\gamma^{\text{obs}}(E_{\text{S}}) = p_0 \cdot (\log(E_{\text{S}}) + p_1)^{p_2}. \tag{5.4}$$

Applying this to the simulated data gives the parameters shown in table 5.7.

E_{thr}[eV]	p_0	p_1	p_2	Valid for energies [eV]
10^{17}	12.72	19.66	2.828	$10^{19.9} - 10^{23}$
10^{18}	4.55	19.67	2.79	$10^{19.8} - 10^{23}$
10^{19}	1.0	19.71	2.73	$10^{19.8} - 10^{23}$

Table 5.7: Parameters for fitting $_{\text{max}}N_\gamma^{\text{obs}}(E_{\text{S}})$

5.4 Magnetic fields 1D

Apart from the deflection of cosmic rays caused by intergalactic magnetic fields, the charged components of the electromagnetic cascades are also influenced by synchrotron losses in these fields. The effect, these losses have on the energy distance matrix, is investigated here.

For this purpose, the simulation series of the previous section is repeated with two different homogeneous transversal magnetic fields with the strength of $0.1\,\text{nG}$ and $1\,\text{nG}$. This field strength is in the order of the average magnetic field strength

(a) $E_{\text{thr}}{=}10^{18}\,\text{eV}$ (b) $E_{\text{thr}}{=}10^{17}\,\text{eV}$ (c) $E_{\text{thr}}{=}10^{19}\,\text{eV}$
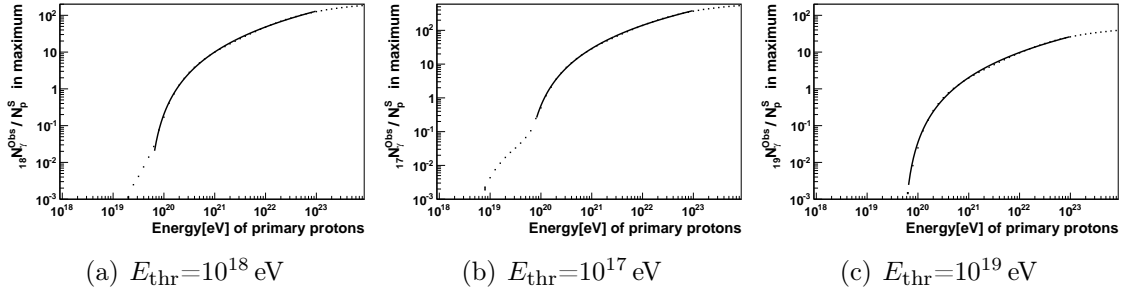
Figure 5.7: The points show $_{\max}N_\gamma^{\text{obs}}$ in dependence of E_{S} for the simulation series with primary protons. The black line shows he parameterization of this values.

derived by some simulations as mentioned in chapter 3. To lower the computational effort a less dense distance grid and a shorter source energy range from $10^{18}\,\text{eV}$ to $10^{22}\,\text{eV}$ is used. Moreover, the statistics is limited to 50000 protons emitted from each source for the whole simulation series.

5.4.1 Results

The resulting $^{N_\gamma^{\text{obs}}}/_{N_{\text{p}}^{\text{src}}}$ ratio for these two series are shown in figure 5.8. To point out the effect of magnetic fields, the ratio $(N_{\text{magnetic field}}^{\text{threshold}}/N^{\text{threshold}})$ of the values in figure 5.8 and the corresponding values in figure 5.1 for the simulation series without magnetic fields in section 5.3 is depicted in figure 5.9 for the three different energy thresholds for the observed photons. One can see, that due to the synchrotron radiation, a reduced $^{N_\gamma^{\text{obs}}}/_{N_{\text{p}}^{\text{src}}}$ ratio is detected at the observer especially for larger source distances and higher proton energies at source. The maximum deficit for example for photons above $10^{18}\,\text{eV}$ is 94% for the 0.1 nG field and 98% for the 1 nG field, which appear for the highest simulated source energies of $10^{22}\,\text{eV}$ and a source distance of about 100 Mpc for both fields. For near distances a slight increase can be observed for high source energies, that is only barely seen in this figure.

5.4.2 Interpretation

As already mentioned the effect here is caused by synchrotron radiation in the magnetic field. The power of this radiation behaves like $P \propto E^2 \cdot B^2$ [26]. This effect accelerates the electromagnetic cascading. For small distances this leads to an increase of the observed photons above the threshold. But for large distances more photons drop under the threshold before the cascade reaches the observer.

(a) $E_{\mathrm{thr}}= 10^{17}$ eV   (b) $E_{\mathrm{thr}}=10^{18}$ eV   (c) $E_{\mathrm{thr}}=10^{19}$ eV

(d) $E_{\mathrm{thr}}=10^{17}$ eV   (e) $E_{\mathrm{thr}}=10^{18}$ eV   (f) $E_{\mathrm{thr}}= 10^{19}$ eV
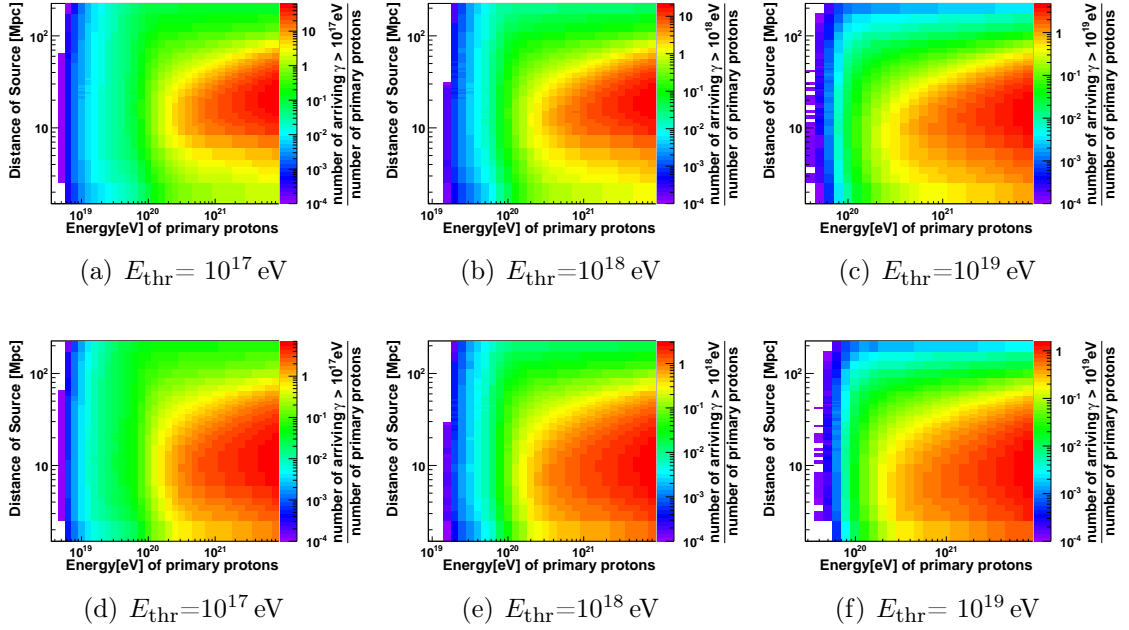
Figure 5.8: $N_\gamma^{\mathrm{obs}}/N_{\mathrm{p}}^{\mathrm{src}}$ of the simulation series with magnetic fields (0.1nG in the first row and 1nG in the second row)

(a) threshold 10^{17} eV   (b) threshold 10^{18} eV   (c) threshold 10^{19} eV

(d) threshold 10^{17} eV   (e) threshold 10^{18} eV   (f) threshold 10^{19} eV
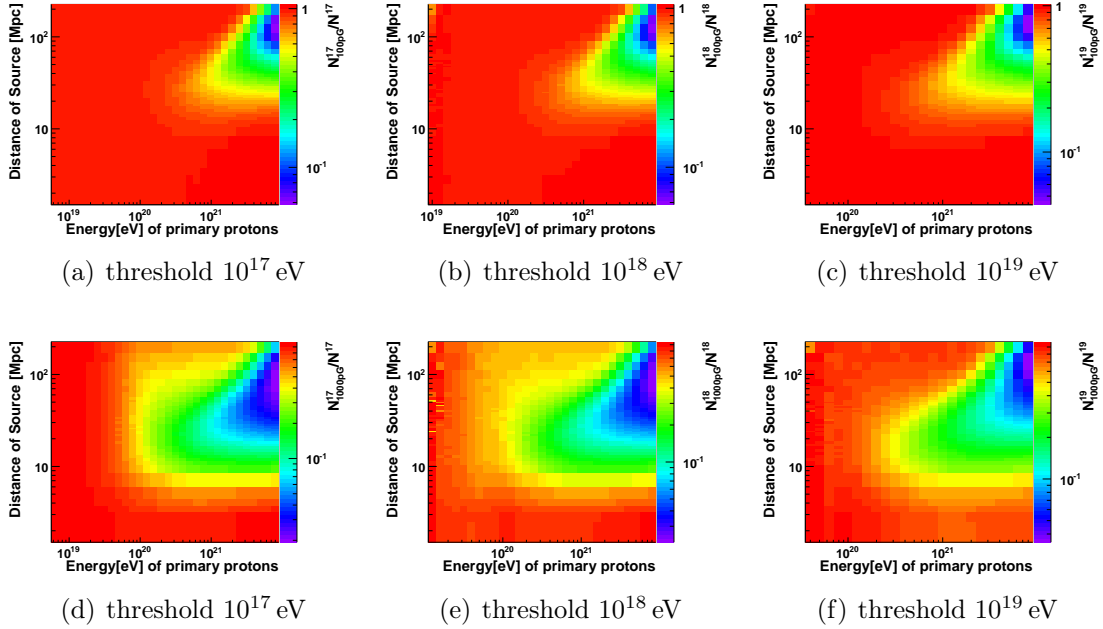
Figure 5.9: Ratio of $N_\gamma^{\mathrm{obs}}/N_{\mathrm{p}}^{\mathrm{src}}$ of the simulation series with a magnetic fields (0.1nG in the first row and 1nG in the second row) to the one without magnetic fields

5.5 Only Pair Production

One interesting additional question is how the results for the energy distance matrix change without the GZK-effect, so that electromagnetic cascades are only induced from proton pair production process. The amount of statistics and the energy distance grid is the same as in section 5.4. The resulting $N_\gamma^{\mathrm{obs}}/N_{\mathrm{p}}^{\mathrm{src}}$ ratio is shown in figure 5.10. The maximum entries are by a factor of thousand smaller than in the case of a combination of pion production and pair production. The energy loss length of pair production is always larger than 1000 Mpc as shown in figure 4.1. Because of this the protons should initiate electromagnetic cascades in the whole observed distance range and the photon number should increase continuously, as it is seen.

(a) $E_{\mathrm{thr}}=10^{17}$ (b) $E_{\mathrm{thr}}=10^{18}$ (c) $E_{\mathrm{thr}}=10^{19}$
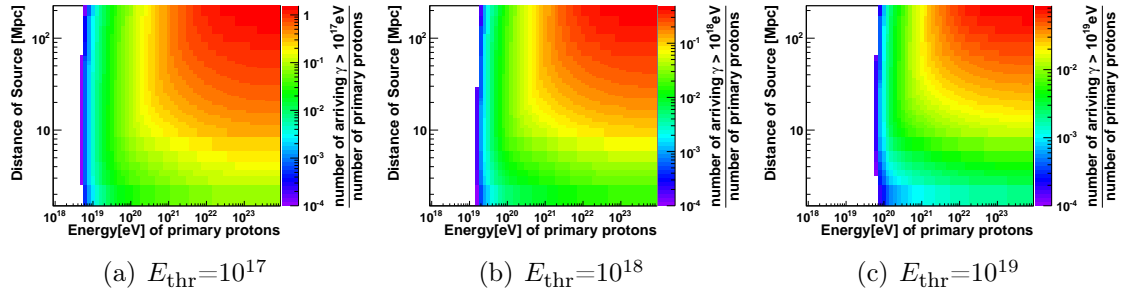
Figure 5.10: $N_\gamma^{\mathrm{obs}}/N_{\mathrm{p}}^{\mathrm{src}}$ of the simulation series with only pair production as interaction for protons

6 Studies with a three dimensional propagation model

6.1 Aim

In this chapter different studies are performed with the three dimensional simulation mode of CRPropa. The main advantage of this propagation model compared to the one dimensional mode is the possibility to take into account the deflections of charged cosmic rays in intergalactic magnetic fields. To study this influence on the cosmic ray propagation, we regard the scenario of point sources which emit ultrahigh energy protons isotropically. The main information of interest is how the arriving direction of UHE nucleons and photons at Earth like observers deviates from the direction of the source. From now on the two corresponding angles are named φ_n and φ_γ, respectively. Especially the relation of these two angles for UHE particles above different energy thresholds (E_{thr}) will be investigated for different source parameters and magnetic field assumptions.

The UHE photon component is purely produced during the propagation of nucleons through interactions with the low energy photon background. As mentioned in chapter 4 the electromagnetic cascades, in which the UHE photons propagate, experience only negligible deflections in magnetic fields. Therefore in CRPropa they are only propagated in straight lines. So the angle φ_γ is only influenced by the direction of the nucleon that produced the electromagnetic cascade. These nucleons have in average traveled smaller distances than those nucleons, that hit the observer. This leads to the assumption, that observed UHE photons should point back more to the source, than the observed nucleons.

Based on the CRPropa Monte Carlo code, the validity of this assumption is analyzed and quantified.

6.2 General preparations

6.2.1 Angular resolution of detecting mechanism

Obviously the detection of a particle needs an extended observer, which is realized in CRPropa by a sphere centered at the position of the observer. Every time a nucleon or a secondary particle hits this sphere, its current properties are recorded.
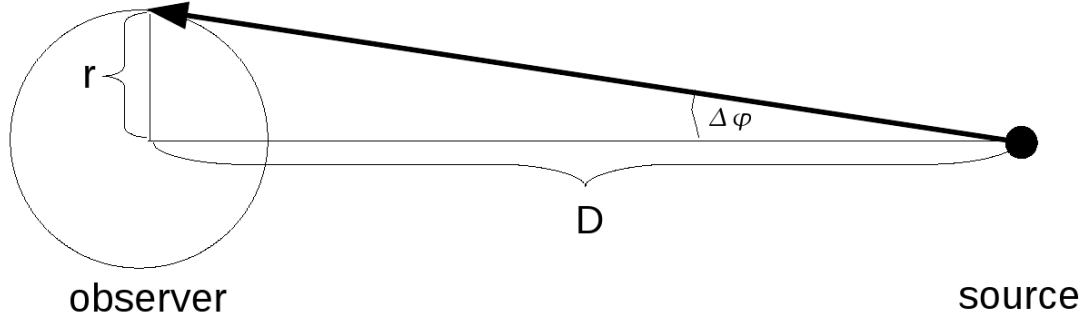
Figure 6.1: Sketch for describing the maximum uncertainty, due to the detecting mechanism in CRPropa

This detecting mechanism also causes an uncertainty in the arrival direction of the detected particles, because of different impact parameters as one can see in figure 6.1. The maximum departure, is given by

$$\Delta\varphi_{\max} = \arctan\frac{r}{D}, \tag{6.1}$$

where r is the radius of the observer sphere and D the distance from the center of the observer to the source. For a source distance of $3\,\mathrm{Mpc}$, which is of the order of the minimum distance used in this chapter, this means a $\Delta\varphi_{\max}$ of $1.91°$, $0.91°$ and $0.38°$ for observer radii of $0.1\,\mathrm{Mpc}$, $0.05\,\mathrm{Mpc}$ and $0.02\,\mathrm{Mpc}$ respectively. A few test

(a) r=0.1 Mpc, D=3 Mpc

(b) r=0.05 Mpc, D=3 Mpc

(c) r=0.02 Mpc, D=3 Mpc
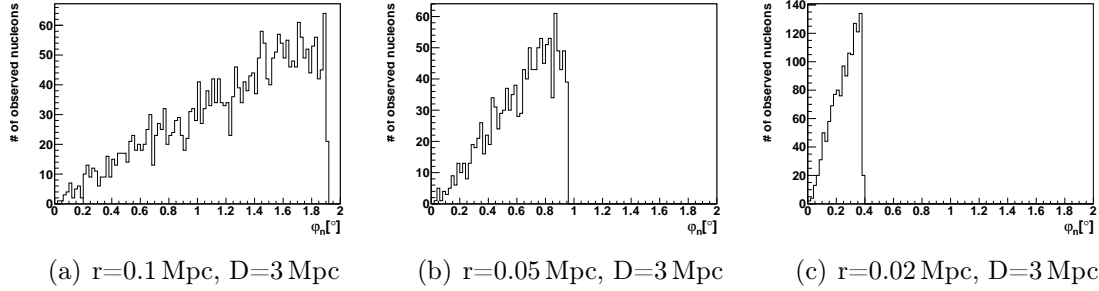
Figure 6.2: φ_n distribution, that shows the systematic uncertainties introduced by the observer sphere for different sizes of this sphere for test simulations with a fix source distance of $3\,\mathrm{Mpc}$

simulations are run in the absence of magnetic fields and no interactions to confirm this assumption. In each of these simulations, a single point source, that emits protons with a discrete energy of $10^{18}\,\mathrm{eV}$, is placed in a distance of $3\,\mathrm{Mpc}$ from the observer whereupon the radius of the observer is one of the above mentioned values. The corresponding φ_n distributions in figure 6.2 are in good agreement with the

calculated values. Furthermore one can see that the number of events increases with φ_n. The explanation for this is, that for bigger impact parameters, the corresponding area on the surface of the sphere grows and thus also the probability for a nucleon to hit the sphere.

As an acceptable size of this uncertainty $\Delta\varphi_{max} = 0.38°$ is chosen, and so an observer radius of $0.02\,\mathrm{Mpc}$. This is sufficient, because this is below the accuracy of measured data for example those of the Pierre Auger Observatory, who have a angular accuracy of about one degree [27]. But with a smaller observer volume the probability for an event to hit the observer is also reduced, $r=0.02\,\mathrm{Mpc}$ is too small for larger source distances, where the statistics has to be increased considerably to gather the same amount of events at source. For this reason, the observer radius is changed with the source distance, so that this systematic uncertainty stays constant according to equation 6.1. Some test simulations with different source distances are done, where this procedure is applied. The resulting φ_n distributions shown in figure 6.3 confirm the effect on these systematic uncertainties.

(a) r=0.02 Mpc, D=3 Mpc   (b) r=0.0667 Mpc, D=10 Mpc   (c) r=0.5 Mpc, D=75 Mpc
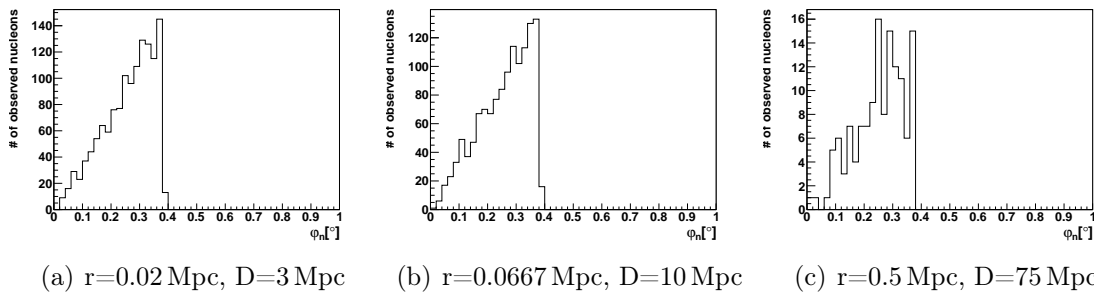
Figure 6.3: φ_n distribution, that shows the systematic uncertainties caused by the observer sphere for simulations with different source distances, where accordantly the observer size is changes to keep the uncertainties constant

Size of simulation box   In chapter 4 it is already mentioned that in the three dimensional mode of CRPropa a fixed propagation volume with periodic boundary conditions is used, whose size have to be specified at the beginning of the simulation. Because one of the main aims of this chapter is to study how many UHE nucleons and photons point back to the sources, periodic boundary conditions are not useful in this case. This feature would cause artificial arrival directions. To prevent this, the size of the simulation box and the maximal propagation time for the nucleons are chosen in such a way that particles reentering due to the boundary conditions can not hit the observer. These two parameters of the simulation are chosen individually in the coming simulation series, as it will be specified in the according sections.

6.3 Homogeneous magnetic field

In this first two simulation series, magnetic fields with the field strength of 1 nG and 10 nG, which are both homogeneous in the whole simulation box, are used respectively. Both fields are directed perpendicular to the straight line through source and observer.

Consequently, the nucleon trajectories are expected to be helixes around the magnetic field lines[1] intermittent by short straight lines for the neutron phases. Although this is not a very realistic scenario, this magnetic field allows a good prediction of the expected effects they cause on cosmic ray propagation. The first question is, how the φ_n and φ_γ distributions for particles with energies above different energy thresholds vary with the energy of the corresponding source protons and the distance to the source. To study this, protons which have energies (E_S) at the source between $10^{18.5}$ eV and 10^{22} eV and following an E^{-1} spectra are simulated for the four source distances 3.9 Mpc, 10 Mpc, 40 Mpc and 75 Mpc. The E^{-1}-spectrum yields that the starting probability for a proton is equal in every order of magnitude of energy. It should be mentioned that in CRPropa the only way to set a lower boundary energy of the injection spectrum is to set the minimum energy of the simulation to this value. Hence, all nucleons, that drop under this threshold are deleted from the simulation. Because of this, the useful minimum threshold energy for the observed particles is this lower boundary energy.

6.3.1 Preparing the simulation

Size of simulation volume

The size of the simulation box is chosen to be 400 Mpc with the observer placed in the centre of this cube. This is much larger than the largest source distance.

Estimation of the maximum propagation time of the simulation

Test simulations with this magnetic field, where all interactions are switched off and only protons of one discrete energy are submitted by one point source, show two different arrival directions for the nucleon events. One with a φ_n smaller (trajectory a) and one bigger (trajectory b) than 90°. This is a result of simple geometry. For a circular trajectory, whose diameter is larger than the distance between source and observer two starting directions are possible, that hit the observer like shown in the sketch in figure 6.4. This effect is also visible in the distribution of the propagation times as shown in figure 6.4(b). As one would not expect such huge homogeneous magnetic fields in the Universe, the effect of the trajectory b is not relevant for this

---

[1]helixes and not simply circles, because of the part of the start momentum of the protons, which is parallel to the magnetic field
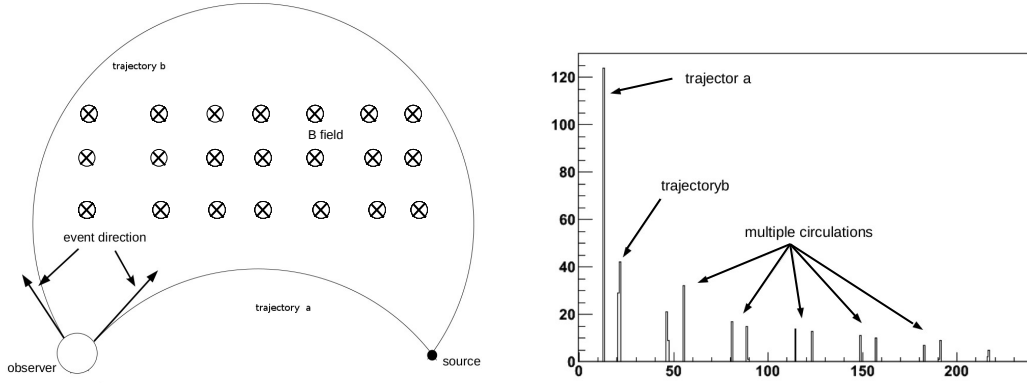
(a) Sketch of possible trajectories for particles with the same energy in a homogeneous magnetic field

(b) Shown is the distribution of the arrival time (in Mpc) of nucleons with an energy of $5 \cdot 10^{18}$ eV, which are emitted from a point source in 10 Mpc distance. The simulation is run with no interactions and in the 1 nG magnetic field

Figure 6.4: Possible nucleon trajectories in a homogeneous magnetic field

studies. Therefore, the maximum propagation time in the simulation is set to the time the lowest energy nucleon, that is able to achieve the observer, would need for its trajectory ($\frac{1}{2}\pi \cdot D$). The trajectory b should be larger than this distance for all nucleons with higher energies and should prevent them to hit the observer. As a consequence only deflections up to 90° should be observed.
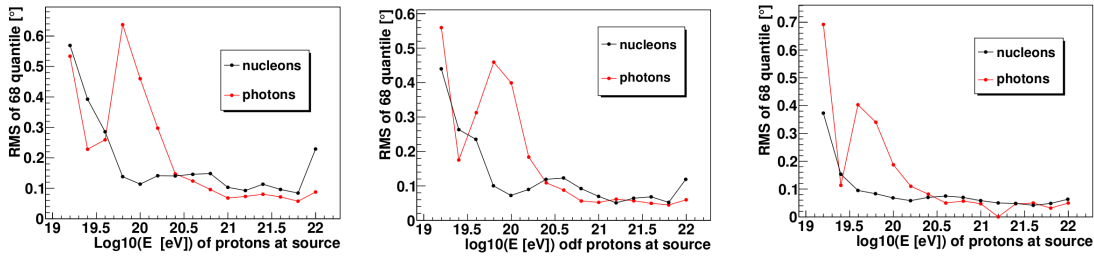
(a) 50 million primary protons   (b) 100 million primary protons   (c) 200 million primary protons

Figure 6.5: Test of the fluctuations of the 68-quantile values of φ_n and φ_γ for different numbers of primary protons started in one simulation

Estimation of the amount of statistic needed in the simulation

As in chapter 5 the amount of statistics which is necessary to keep the fluctuations of the quantities of interest small, have to be estimated. The main quantity of interest

from the simulations in this chapter will be the 68-quantile values of the distributions of the already mentioned φ_n and φ_γ values for different source energy ranges, as will be described later in this section. To estimate these fluctuations for a fixed amount of statistics, namely a fixed number of protons starting at the source, the same simulation is repeated with different random seeds, and the mentioned 68-quantile values are determined for each of this simulations. Doing this for a proton source with an E^{-1} energy spectrum at a distance of 10 Mpc from the observer and the 1 nG magnetic field described above provides the results shown in figure 6.5. Here the root mean square (RMS) for the 68-quantile values in dependence of the source energy are shown for a statistics of 200, 100 and 50 million protons starting at the source. The number of simulations within which the RMS values are calculated are 9, 19 and 38, respectively. Because of this, especially the first two estimations of the fluctuation are not very reliable, but more simulations would be too CPU time consuming. This is also the reason, why this method is not applied to the other source distances.

	Source distance [Mpc]	Number of starting protons in million
B=1nG		
	3.9	500
	10	2000
	40	200
	75	130
B=10nG		
	3.9	200
	10	200
	40	50
	75	50

Table 6.1: Statistics used in the different simulation series

However we can take the results in figure 6.5 as an estimation for these uncertainties for the source distance of 10 Mpc. One can see in the graph, that for source energies above $10^{20.2}$ eV the fluctuations are below 0.2° for photons and protons, even for a statistics of 50 million source protons. An increase to a RMS of over 0.6° for photons is clearly observed between source energies between $10^{19.6}$ eV and $10^{20.4}$ eV. This can be lead back to the increase in the energy loss length as one can see in 4.1, that causes a decrease in the photon production. This fluctuation drops below 0.4° for a statistics of 200 million protons, what would be an acceptable fluctuation, as already

mentioned in 6.2.1.

For the source distance of 3.9 Mpc one would expect smaller deflections and because of this also smaller fluctuations, so the same statistics as for D=10 Mpc should also be sufficient for this distance. For the two bigger distances of 40 Mpc and 75 Mpc an increase in φ_n and φ_γ and because of this also an increase for the fluctuations of this values would be expected. So an increased statistics should be used for this source distances. But as this would be to CPU-time consuming, it is decided to take the same statistics or even a reduced statistics to save CPU, especially in the second series with the 10 nG field. The number of starting protons for every simulation is listed in table 6.1. The whole data produced for estimating the fluctuation for the case with D=10 Mpc and B=1 nG can be of course also used for the simulation series, what is the reason for the high statistics in that simulation.

6.3.2 Results

For the first simulation series with a 1 nG magnetic field, the resulting φ_n and φ_γ distributions for nucleons and photons with energies above the threshold of $10^{18.5}$ eV at the observer are shown in figure 6.6 in dependence on E_S for each of the four distances. The logarithmically binned source energy is binned with a size of 0.4 to have enough statistic and only energies from $10^{19.4}$ eV upwards are regarded, since primary protons with lower energies do not produce significant amounts of photons above the given threshold. As for the different distances no uniform starting statistic is used, the observed nucleon and photon numbers are normed to 500 million starting protons.

As expected, the φ_γ distributions in these cases seem to point back more to the source than the ones of φ_n for all source distances and all energies of the source protons. For both distributions, the difference of the arrival directions of the events from the source direction increases with decreasing E_S and increasing source distance.

To quantify the φ_n and the φ_γ distributions for the different E_S bins, the angle for which 68 percent of the particles arrive with angles smaller than this one, called the 68-quantile, is determined as shown in figure 6.7. The entries are connected through straight lines to guide the eye.

The 68-quantile values in these plots confirm the already made statements. For the two nearest distances one can see a nearly complete agreement with the source direction for energies above 10^{21} eV, except to a not vanishing offset of 0.4° for nucleons and photons. This offset is already described in section 6.2.1 and is due to the detecting mechanism. Consequently angels below 0.4° have to be assumed as not deflected. For a distance of 75 Mpc a not monotone decrease with E_S for the photon entries can be observed for E_S around $10^{20.4}$ eV and $10^{20.8}$ eV, whereat for $10^{20.8}$ eV the photon value even exceeds the nucleon one. This behaviour is supposed to be a statistical fluctuation, as in this simulation the lowest number of starting protons is used, which one can see in table 6.1 .

(a) φ_n distribution, D=3 Mpc

(b) φ_γ distribution for the, D=3 Mpc

(c) φ_n distribution, D=10 Mpc

(d) φ_γ distribution, D=10 Mpc

(e) φ_n distribution, D=40 Mpc

(f) φ_γ distribution, D=40 Mpc

(g) φ_n distribution, D=75 Mpc

(h) φ_γ distribution, D=75 Mpc
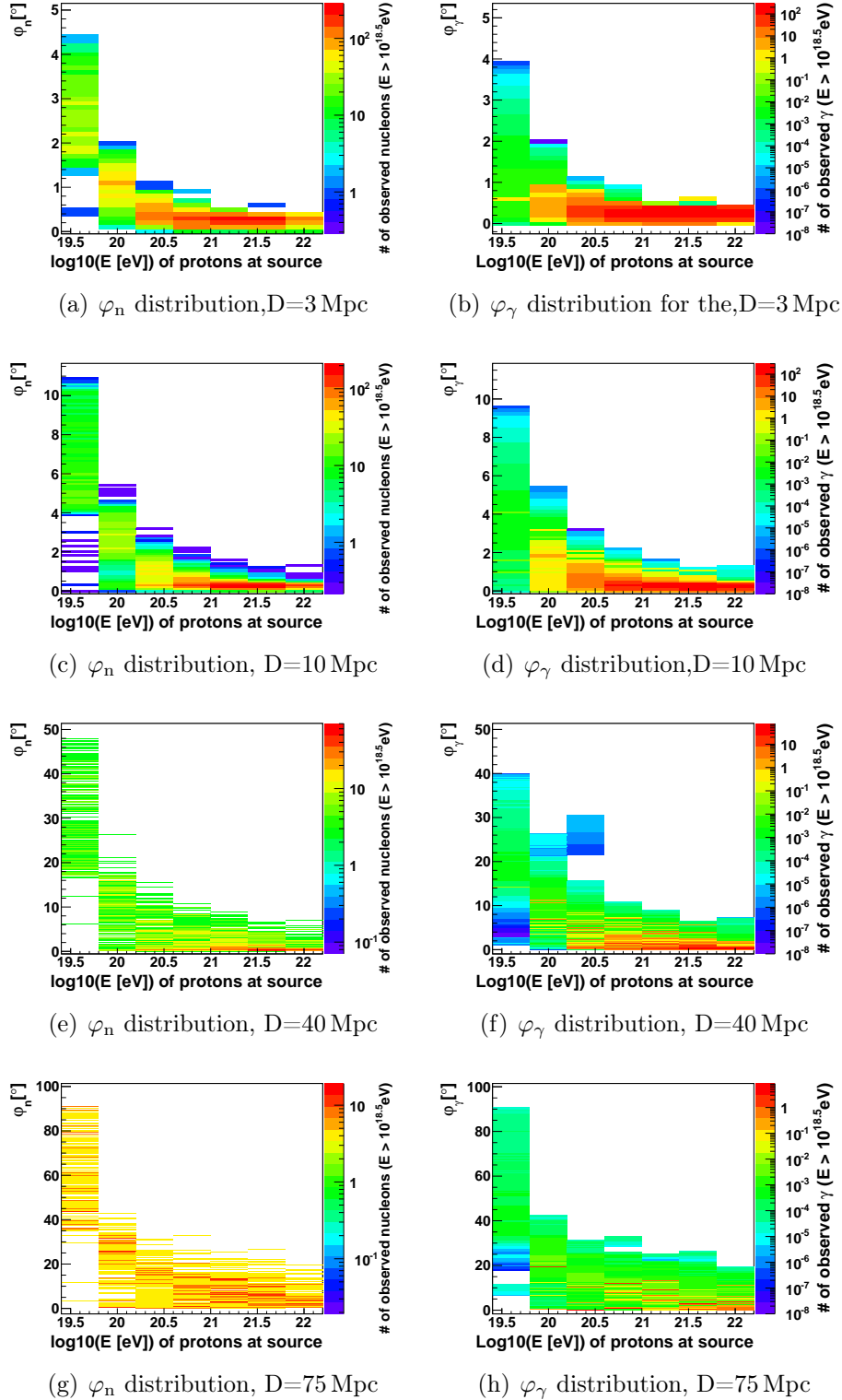
Figure 6.6: φ_n and φ_γ distributions for particle energies at the observer above the threshold of $10^{18.5}$ eV and a homogeneous magnetic field of $1\,\mathrm{nG}$ in dependence of the energy of the primary protons for different source distances

For a quantitative comparison of the point back behaviour of photons to that of nucleons, the ratio of the 68-quantile value for φ_γ to that of φ_n is calculated for each E_S region as shown in figure A.1 in the appendix. Because of the mentioned uncertainties, no reliable conclusions can be taken from this values in general. But to give a rough feeling for this ratio, it can be calculated for the distance of 10 Mpc and E_S of 10^{20} eV, where the statistical and systematical uncertainties should be small. Here this ratio is 0.59.

(a) D=3.9 Mpc

(b) D=10 Mpc

(c) D=40 Mpc
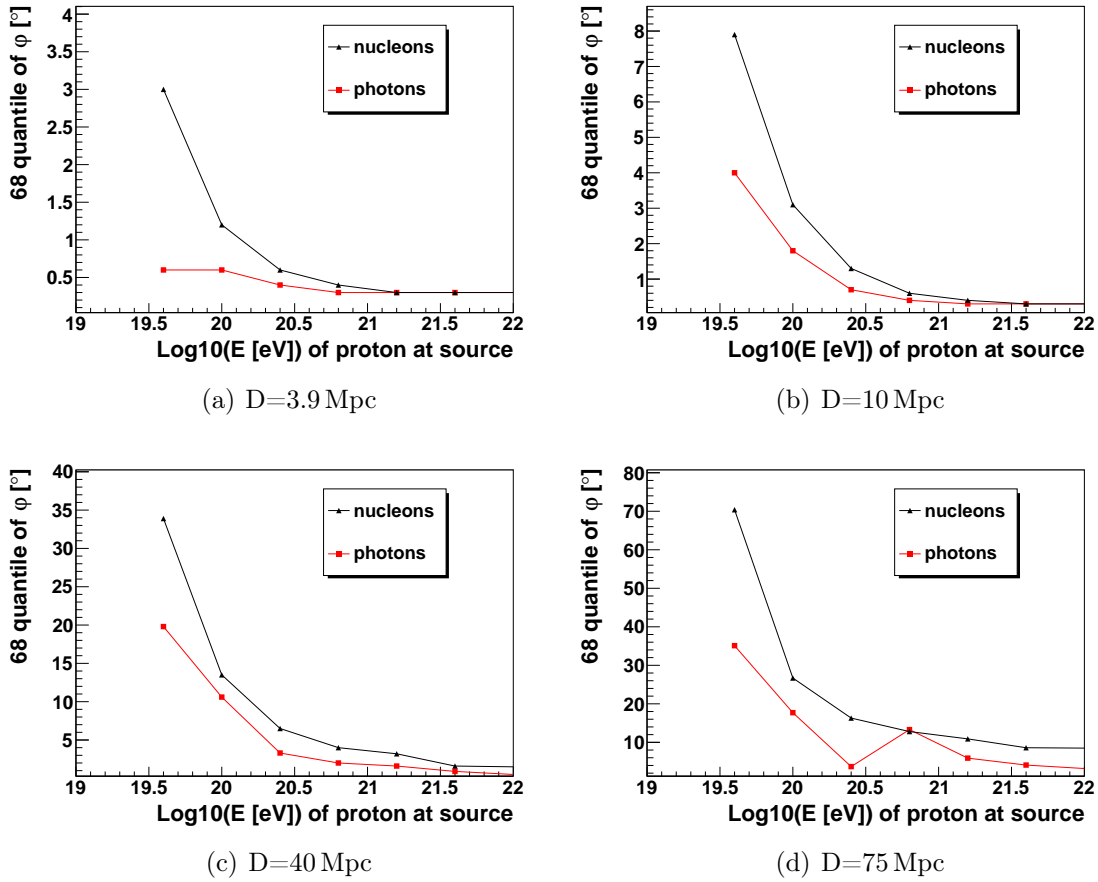
(d) D=75 Mpc

Figure 6.7: 68-quantile for the φ_γ (red) and the φ_n (black) distribution for observed particles with energies above $10^{18.5}$ eV in dependence of the energy of the primary protons for the source distances of 3.9 Mpc, 10 Mpc, 40 Mpc and 75 Mpc and a homogeneous magnetic field of 1 nG

Regarding the effect of different threshold energies at observer

In a next step it is analyzed how the variation of the threshold energy which sets the lower limit for the regarded events affects the hithereto made observations. For

(a) D=3.9 Mpc, $E_{thr}=10^{18.5}$ eV   (b) D=3.9 Mpc, $E_{thr}=10^{19}$ eV   (c) D=3.9 Mpc, $E_{thr}=10^{20}$ eV

(d) D=10 Mpc, $E_{thr}=10^{18.5}$ eV   (e) D=10 Mpc, $E_{thr}=10^{19}$ eV   (f) D=10 Mpc, $E_{thr}=10^{20}$ eV

(g) D=40 Mpc, $E_{thr}=10^{18.5}$ eV   (h) D=40 Mpc, $E_{thr}=10^{19}$ eV   (i) D=40 Mpc, $E_{thr}=10^{20}$ eV

(j) D=75 Mpc, $E_{thr}=10^{18.5}$ eV   (k) D=75 Mpc, $E_{thr}=10^{19}$ eV   (l) D=75 Mpc, $E_{thr}=10^{20}$ eV
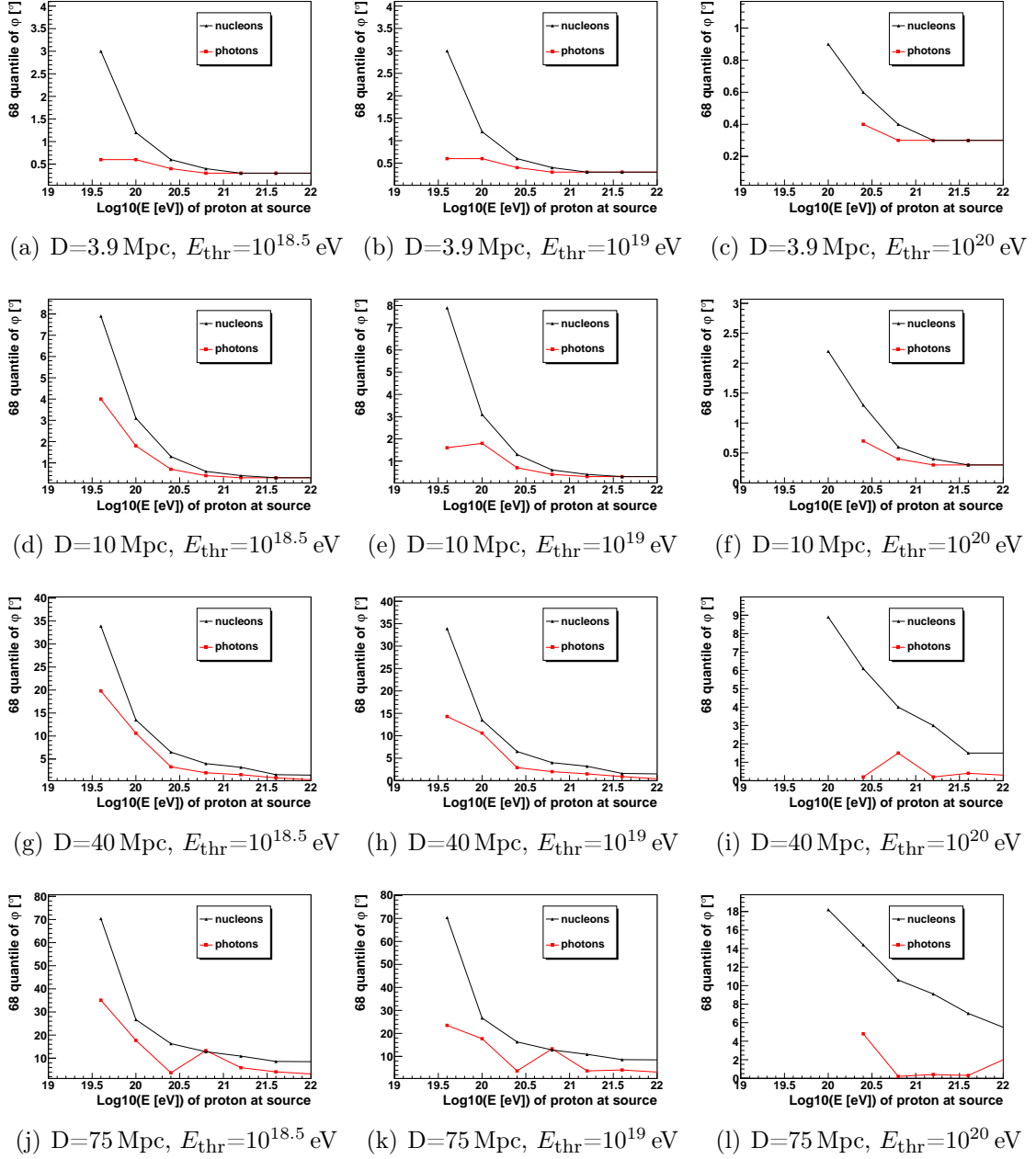
Figure 6.8: 68-quantile for the φ_γ (red) and the φ_n (black) distribution in dependence of the energy of the primary protons for different source distances (columns) and for the different energy thresholds (rows) for a homogeneous magnetic field of 1 nG

this purpose the energy threshold is raised to 10^{19} eV and 10^{20} eV and the results are compared with the previously used threshold of $10^{18.5}$ eV. The comparison of the 68-quantiles are shown in figure 6.8, where every column shows the results for the different source distances for one fixed threshold, which is increased in every row from $10^{18.5}$ eV to 10^{20} eV. In these figures one can see that increasing the threshold reduces the 68-quantile only for the φ_γ distributions, which are induced by protons with source energies close to this threshold. This results from the fact that the energy of the photons created out of the photo-pion production is on average nearly an order of magnitude smaller, than the remaining energy of the nucleon from this interaction. Raising the energy threshold affects therefore more the photon component. Consequently this means that the better point back behaviour of the photons observed here refers to photons with an average much smaller energy than that of the protons, with which they are compared.

Results for the homogeneous magnetic field with 10nG

Regarding the φ_γ and the φ_n distributions for the second simulation series with a homogeneous magnetic field with the strength of 10 nG, shows a similar behaviour as for the previous series with a 1 nG magnetic field for the two nearest distances of 3.9 Mpc and 10 Mpc, as shown in figure 6.9. The difference are of course, that the distributions are shifted to larger values, as is seen in figure 6.10.

For the two more remote distances of 40 Mpc and 75 Mpc only single arbitrary distributed entries can observed for protons asit is seen in figure 6.9. The fact, that the graphs shows entries of ten results from normalization mentioned in section 6.3.1. This is because of the too large distance of these sources. Most nucleons are deflected too strong in the magnetic field to reach the observer.

Unexpected photon entries

Unexpected structures occur in the φ_γ distributions as one can see in figure 6.11. Here very few entries for high source energies and large angles appear, which are not expected. Although these few entries should not have any significant effect on the results of the simulation, their existence should be mentioned. One possible reason for this structure could be the periodic boundary conditions of the simulation box. Although the maximum propagation time of the photons is set to inhibit the detection of reentered nucleons, photons produced during the nucleon propagation can not be bound to this constrain and therefore can reach the observer. One could control this assumption by enlarging the simulation volume, which should lower these entries. This would then also be a method to prevent these unwanted detections.

(a) φ_n distribution, D=3.9 Mpc

(b) φ_γ distribution, D=3.9 Mpc

(c) φ_n distribution, D=10 Mpc

(d) φ_γ distribution D=10 Mpc

(e) φ_n distribution, D=40 Mpc

(f) φ_γ distribution, D=40 Mpc

(g) φ_n distribution, D=75 Mpc

(h) φ_γ distribution, D=75 Mpc
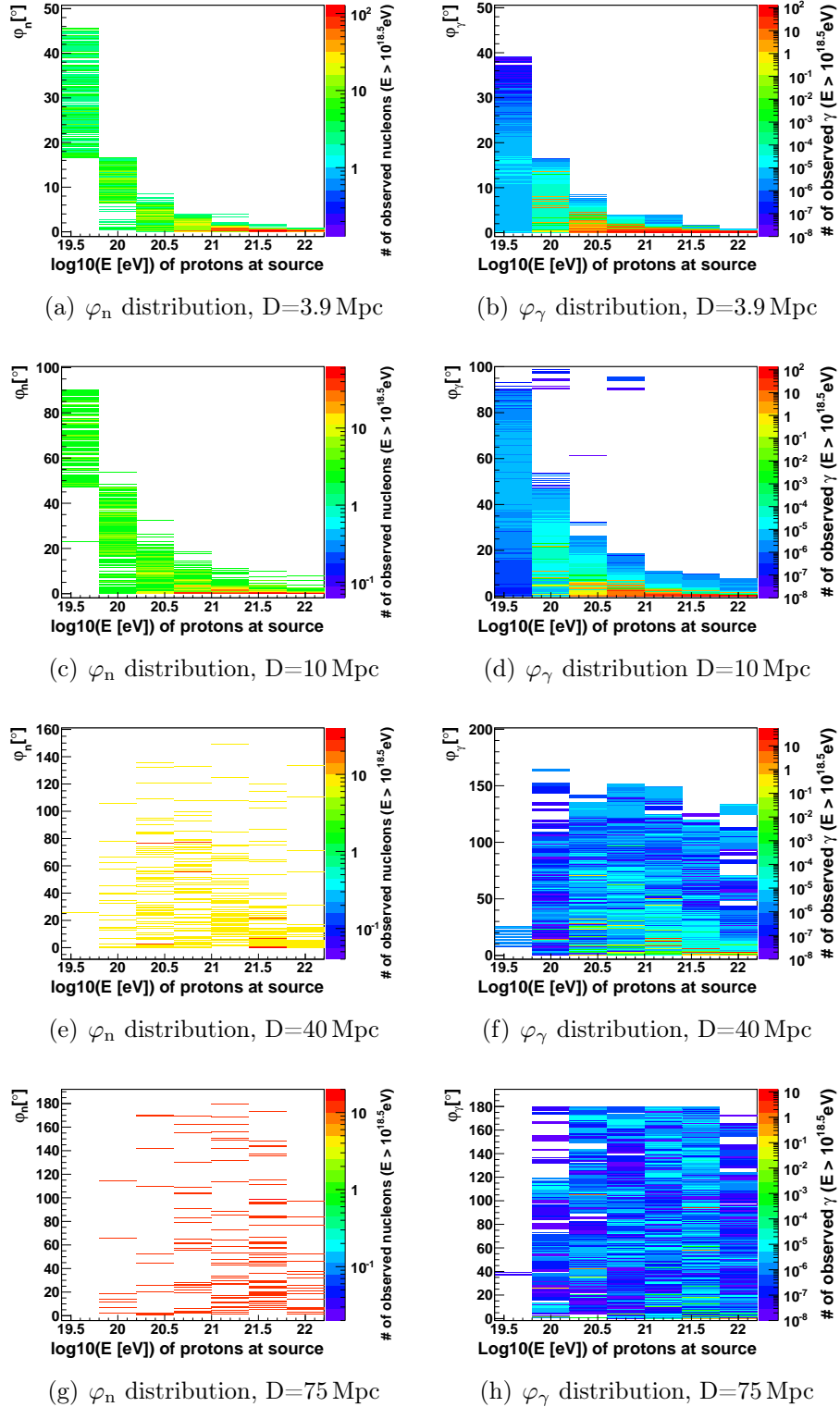
Figure 6.9: φ_n and φ_γ distributions in dependence of the energy of the primary protons for source distances of 3.9 Mpc, 10 Mpc and 75 Mpc by and a homogeneous magnetic field of 10 nG

(a) D=3.9 Mpc, B=1 nG

(b) D=10 Mpc, B=1 nG

(c) D=3.9 Mpc, B=10 nG

(d) D=10 Mpc, B=10 nG
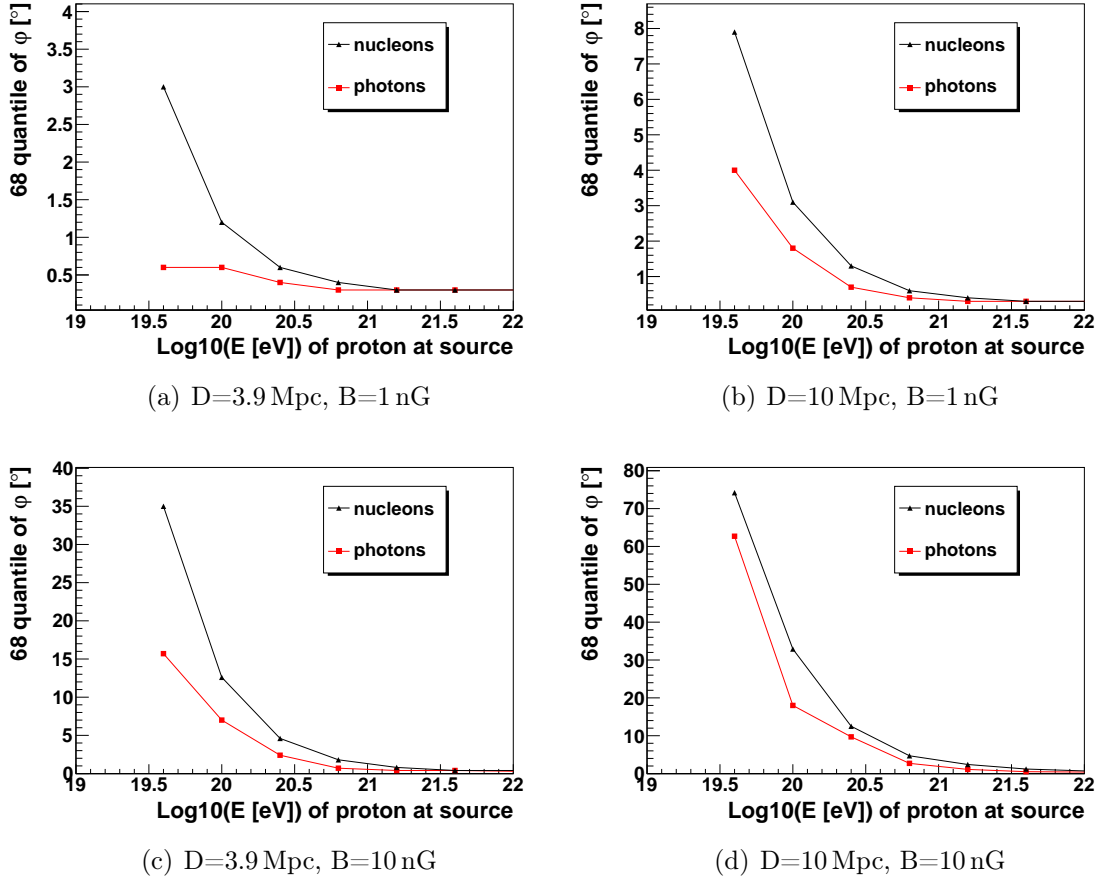
Figure 6.10: 68-quantile for the φ_γ (red) and the φ_n (black) distribution for observed particles with energies above $10^{18.5}$ eV in dependence of the energy of the primary protons for the source distances of 3.9 Mpc and 10 Mpc and a homogeneous magnetic field of 1 nG (first row) and 10 nG (second row)

(a) D=3.9 Mpc   (b) D=75 Mpc
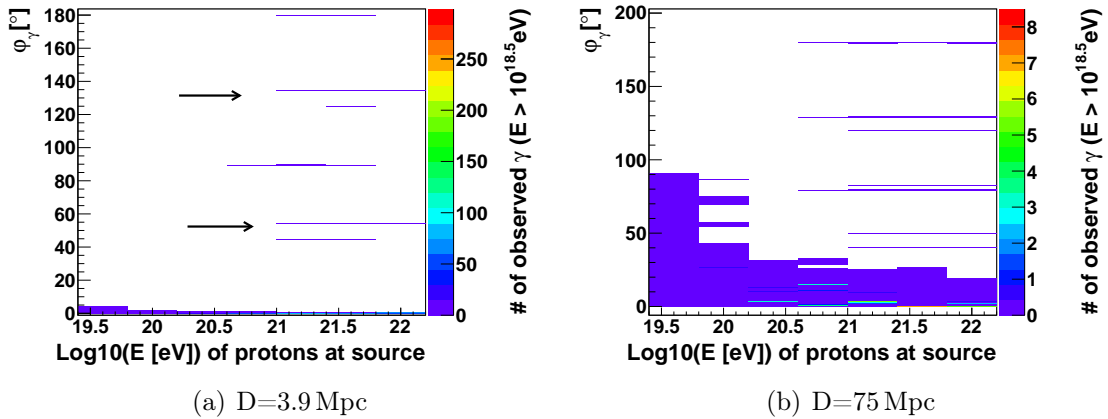
Figure 6.11: The two figures show unexpected photon entries for different φ_γ values

6.3.3 Energy spectrum of E^{-2}

The next question that arises, is how the φ_n and φ_γ distributions look like for the whole energy spectrum of source protons for the homogeneous magnetic field scenario. Therefore, the output of the already simulated E^{-1} source spectra is reweighted to get the results of an E^{-2} spectra, which is the result for a source of UHECR in an acceleration scenario. The resulting φ_n and φ_γ distributions for nucleons and protons above a threshold energy of $10^{18.5}$ eV and an end of the source energy spectrum at $E_{cut}=10^{20.5}$ eV, which matches the highest observed cosmic ray events, as described in chapter 2.1, are shown in figure 6.12. For this threshold in fact no correlation with the arrival direction can be seen for nucleons, whereas the φ_γ distribution for photons above this energy show a clear directional correlation, even for the largest observed source distance of 75 Mpc. The extreme large φ_n angle is caused by the protons of lowest energies, that were not regarded till now, as mentioned above. The maximum values of the arrival direction of 90° is due to the setting of the maximal propagation time as described in section 6.3.1.

For a better comparison of this distributions, again the 68-quantile is determined for each source distance. The resulting values are shown in figure 6.13(a). The 68-quantile for the φ_n is saturated at about 60° that corresponds to 68% of the 90°. The 68-quantile for the φ_γ even for this low thresholds stays below 20°. One can see that the 68-quantile for the φ_γ distribution seem to be in good agreement with the values from the previous section.

Increasing the lower threshold for the observed particles to 10^{19} eV and 10^{20} eV as shown in the first column of figure 6.13 lowers the 68-quantiles for both particle types and for all distances, which matches the exceptions. But for even the highest regarded threshold of 10^{20} eV the 68-quantiles for φ_n are at least twice as large as those for the φ_γ. The decrease for photon entries at 75 Mpc in figure 6.13(f) is

due to a lack of statistics, as already discussed in the previous section and not an effect of physics. Raising the highest energy of the spectrum to 10^{22} eV shifts only the 68-quantile of the φ_γ distribution to smaller angles. This effect can be explained with the enhanced production of UHE photons for the proton energies, which are added with the rise of the cut off energy as described in section 5.3. These nucleons themselves seem not to have a significant effect on the φ_n distribution. This seems reasonable because of their low appearance due to the E^{-2} spectra.

(a) D=3.9 Mpc

(b) D=3.9 Mpc

(c) D=10 Mpc

(d) D=10 Mpc

(e) D=40 Mpc

(f) D=40 Mpc

(g) D=75 Mpc

(h) D=75 Mpc
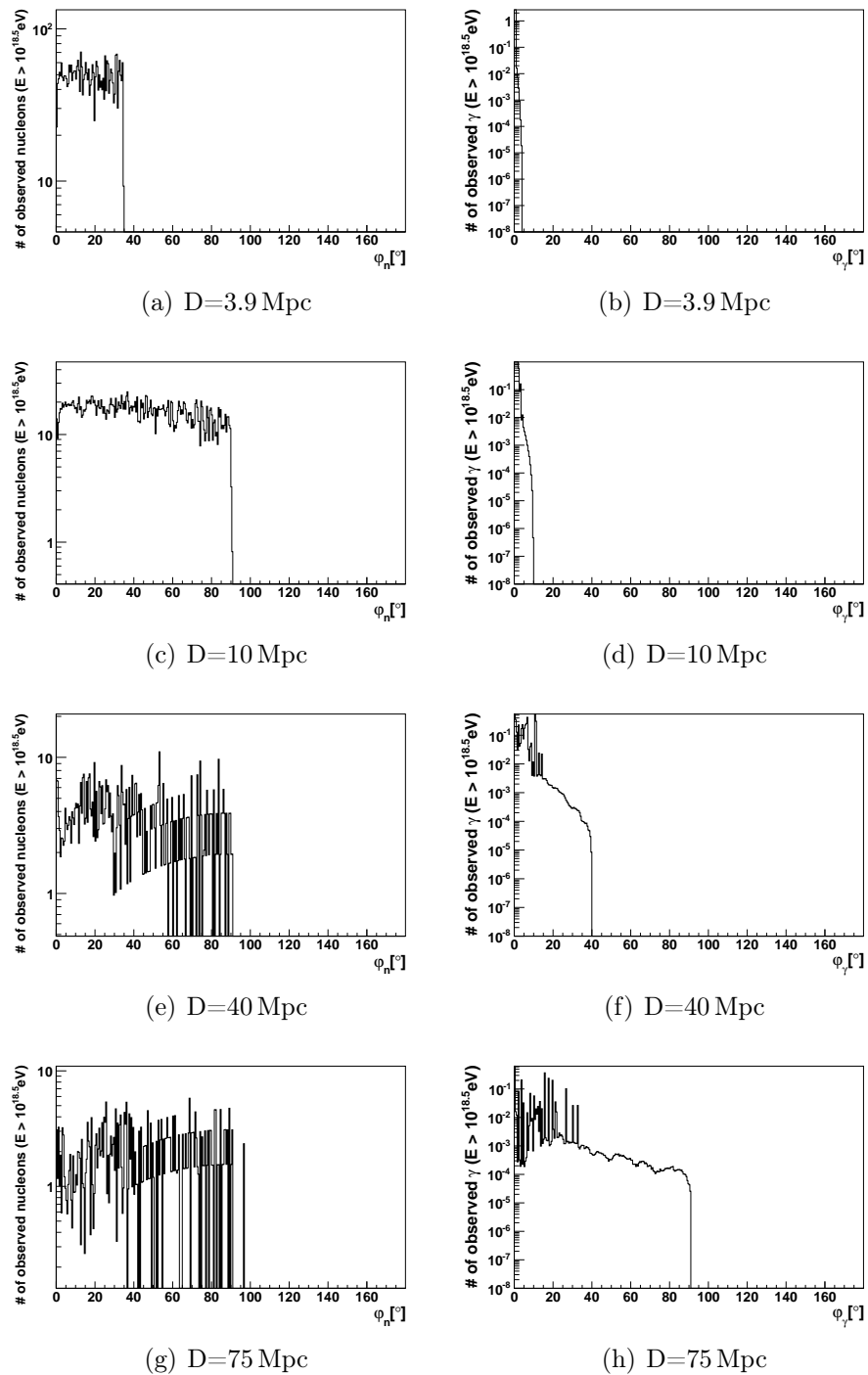
Figure 6.12: The φ_n (left) and φ_γ (right) distribution assuming a homogeneous magnetic field of 1 nG and an E^{-2}-spectrum at source, for the energy thresholds of $10^{18.5}$ eV and a cutoff energy of $10^{20.5}$ eV

(a) $E_{\text{cut}}=10^{20.5}$ eV, $E_{\text{thr}}=10^{18.5}$ eV

(b) $E_{\text{cut}}=10^{22}$ eV, $E_{\text{thr}}=10^{18.5}$ eV

(c) $E_{\text{cut}}=10^{20.5}$ eV, $E_{\text{thr}}=10^{19}$ eV

(d) $E_{\text{cut}}=10^{22}$ eV, $E_{\text{thr}}=10^{19}$ eV

(e) $E_{\text{cut}}=10^{20.5}$ eV, $E_{\text{thr}}=10^{20}$ eV

(f) $E_{\text{cut}}=10^{22}$ eV, $E_{\text{thr}}=10^{20}$ eV
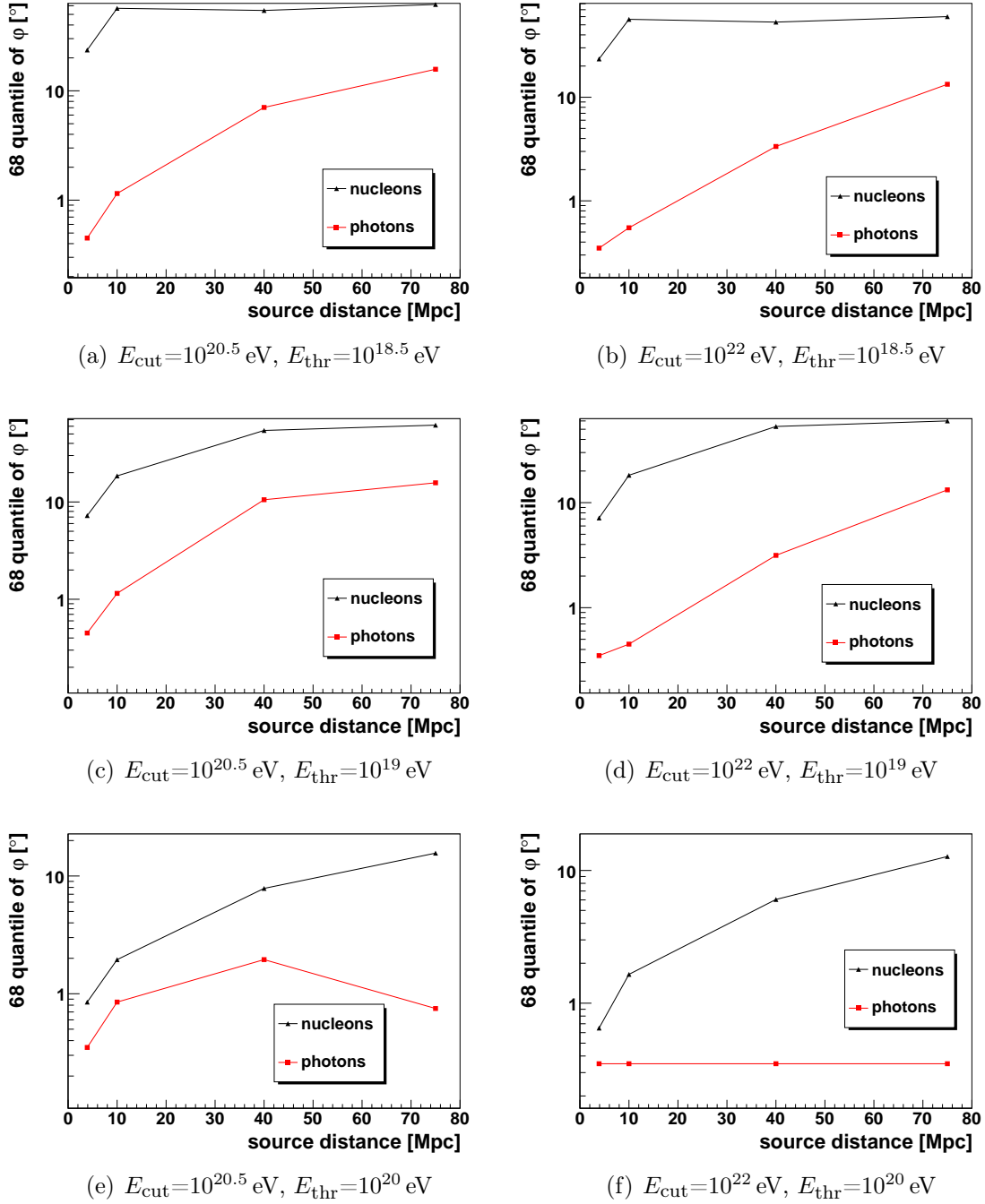
Figure 6.13: 68-quantile for the φ_γ (red) and the φ_n (black) distribution in dependence of the distance of the source assuming a homogeneous magnetic field of 1 nG and an E^{-2}-spectrum at source, for the different energy thresholds of $10^{18.5}$ eV, 10^{19} eV and 10^{20} eV and cutoff energies of $10^{20.5}$ eV and 10^{22} eV

6.4 Structured magnetic field

In this last simulation series a structured three dimensional magnetic field map from the simulations of Miniati et al. [16] is used. In this magnetic field, the results of simulations of single point sources strongly depend on the local structure of the field between the source and the observer. As described in chapter 3 the positions of the magnetic field structures in this map are not correlated with large scale structures in our Universe. Because of this, the results of single point sources would not give a valuable information. Instead, it is more reasonable to regard the mean behaviour for a lot of point sources located at different positions.

In this simulation series, 23 single point sources are distributed in the simulation volume, all at a distance of 10 Mpc to the observer. The energy spectrum at each source follows again an E^{-1} spectrum with an energy range from 10^{18} eV to 10^{22} eV. The observer is positioned in the point with the coordinates (3.79 Mpc, 41.7 Mpc, 45.5 Mpc) shown in figure 6.15 (where it corresponds to the grid points (13, 143, 156)), where the intergalactic magnetic field shows similar strength as in the surrounding of the milky way [28].

6.4.1 Preparations

Maximum CPU time of the simulation

For this simulation series the maximum propagation time for a nucleon in the simulation for which it is not affected by the periodic boundary conditions of the simulation box as described in 6.2.1 is given trough the size of the simulation box, which is 74.6 Mpc. Using such a long propagation time would also need a long computation time. As one can seen in figure 6.14, the gain in the number of detected events decreases rapidly with the propagation time. For this reason it is decided to set the propagation time to 40 Mpc/c.
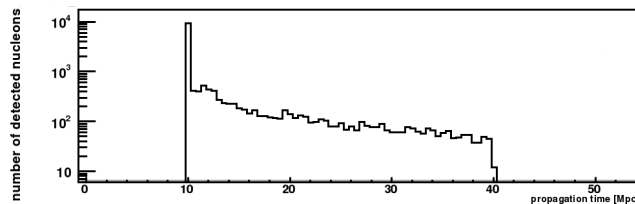
Figure 6.14: Arrival time of the nucleons

(a) $z=45.5\,\mathrm{Mpc}$

(b) $z=35.5\,\mathrm{Mpc}$

(c) $z=55\,\mathrm{Mpc}$
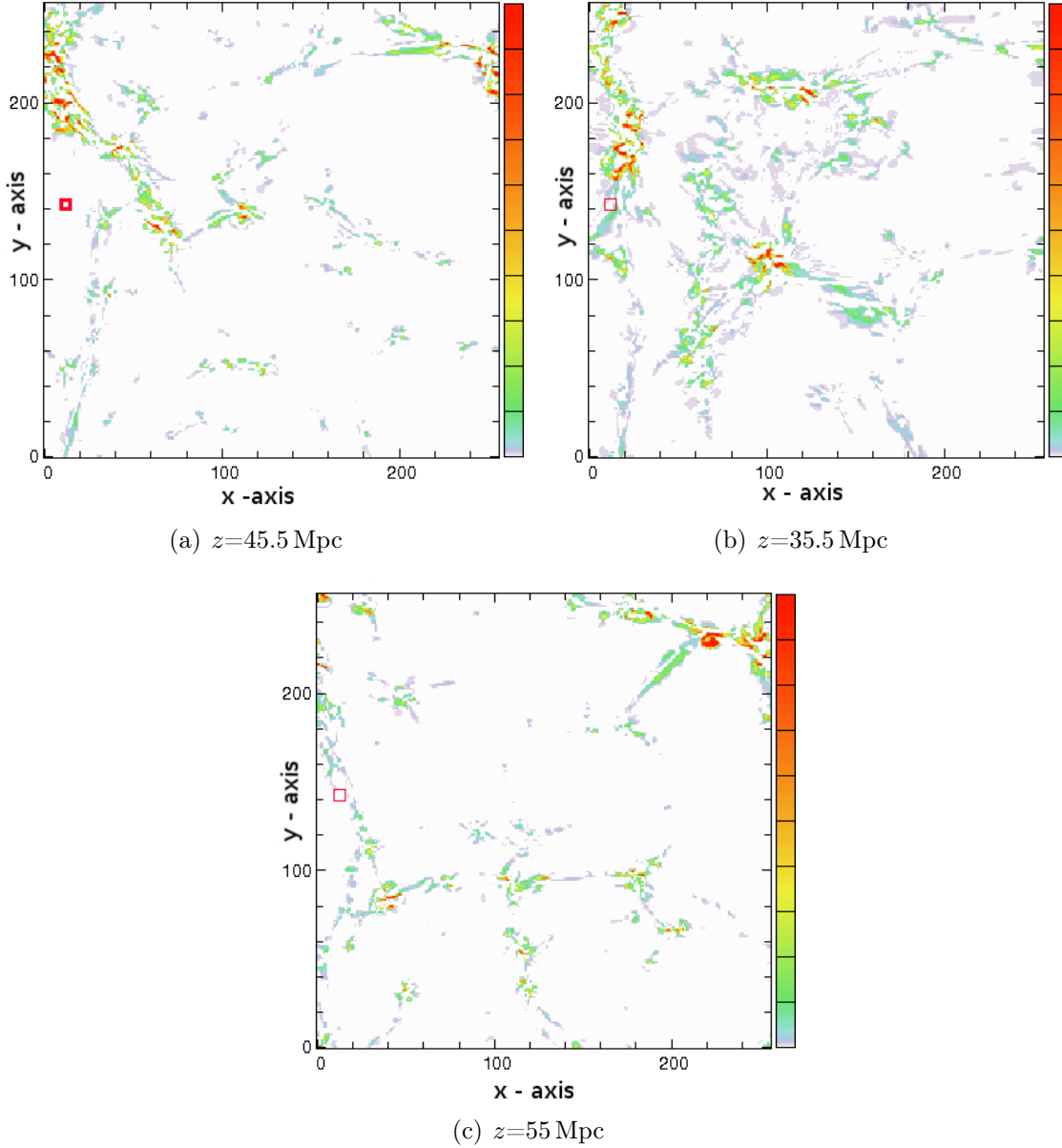
Figure 6.15: Three two dimensional B-Field distributions each at fixed z values of 45.5 Mpc, 35.5 Mpc and 55 Mpc through the three dimensional magnetic field from computer simulations by Miniati [16]. The units of the axis are the grid points of the simulation. The distance between two grid points corresponds to 0.2915 Mpc. The colour code represents the relative magnetic field strength in logarithmic scale. The red square in (a) at (13, 143, 156) marks the position of the source used in this section. The red square in the other two maps just point out the x-y-coordinates of the observer.

Statistics

Each of these 23 sources have been set to emit 50 million protons. This was the smallest statistics tested in the case of a homogeneous magnetic field in section 6.3.1. The maximal fluctuations for this statistics was 0.6°. This value is also take as a rough guideline for the used inhomogeneous magnetic field.

6.4.2 Results

As in the previous section, the distribution of arrival directions of nucleons and photons above a threshold energy of 10^{18} eV is regarded in dependence on the energy of corresponding source protons and the 68-quantiles for φ_n and φ_γ are calculated. The combined results of all 23 sources are shown in figure 6.16. The distribution of φ_n in 6.16(a) and φ_γ in 6.16(b) shows a wide spreed to larger angles at lower source energy. In addition, one can observe different structures in both distributions, which may be caused by the structure of the magnetic field. Determination of the 68-quantile of both distributions in dependence on the source energy shows also for this magnetic field in general a better correlation of the arrival directions to the source direction for photons than for nucleons above the energy threshold of 10^{18} eV. One exception can be seen for the entry for the lowest source energies. To estimate the uncertainties of this two 68-quantile values, the φ_γ and φ_n distributions for this source energy bin are shown in figure 6.17. For the φ_γ distribution one can see multiple bins with an excess in the photon number, which indicates a low statistic in this distribution. Because of this the uncertainty of the corresponding 68-quantile value should be big.

Again some odd structures occur for large source energies and large φ_γ angles in the distribution in figure 6.16(b). They show similar shape to the observations made in the previous section, which was assumed to be a consequence of the periodic boundary conditions. This effect seems to be larger in this simulation series. This would support the assumption of the origin of this odd structures, because the simulation box used here is much smaller than in the last two simulation series.

Regarding different threshold energies at observer

Raising the energy threshold for the observed particles, shows the same behaviour as already observed in the case of a homogeneous magnetic field.

Comparing the different magnetic fields

Comparing the energy dependence of the 68-quantile values of the simulation with the structured magnetic field with the two previous simulation series show the lowest deflection for energies higher than $10^{20.4}$ eV for the inhomogeneous field. For lower energies the values of the structured field lies between 1 nG and the 10 nG field.

(a) φ_n distribution

(b) φ_γ distribution

(c) 68-quantile plot
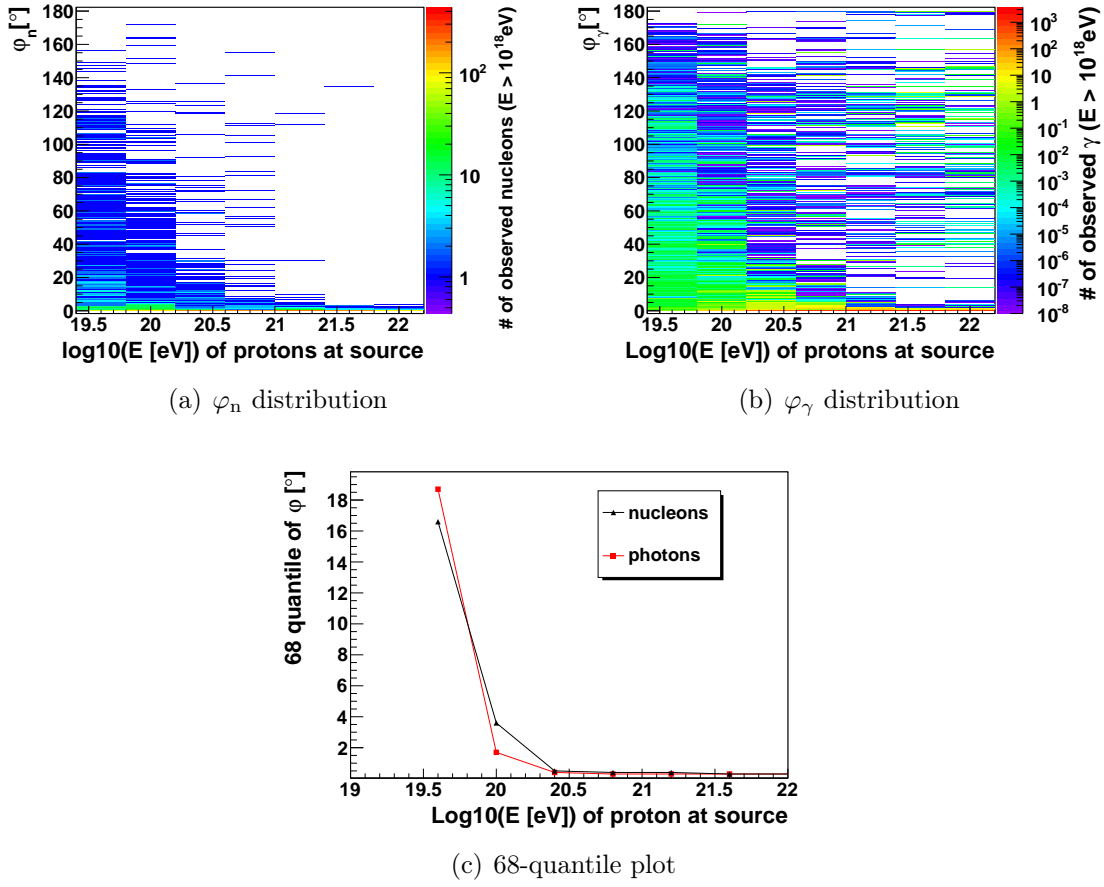
Figure 6.16: φ_n and φ_γ distributions for a threshold energy of 10^{18} eV in dependence on the energy of the primary protons summed for 23 different sources at a distance of 10 Mpc in the Miniati magnetic field.

(a) φ_γ distributions

(b) φ_n distributions
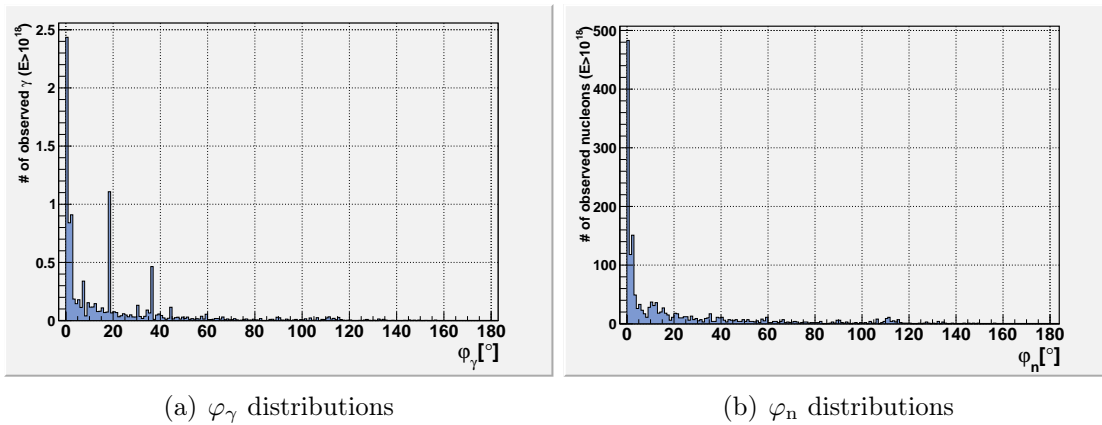
Figure 6.17: φ_n and φ_γ distributions for the source energy of $E_S = 10^{18}$ eV

(a) $E_{\mathrm{thr}}=10^{18}\,\mathrm{eV}$

(b) $E_{\mathrm{thr}}=10^{18.5}\,\mathrm{eV}$

(c) $E_{\mathrm{thr}}=10^{19}\,\mathrm{eV}$

(d) $E_{\mathrm{thr}}=10^{20}\,\mathrm{eV}$
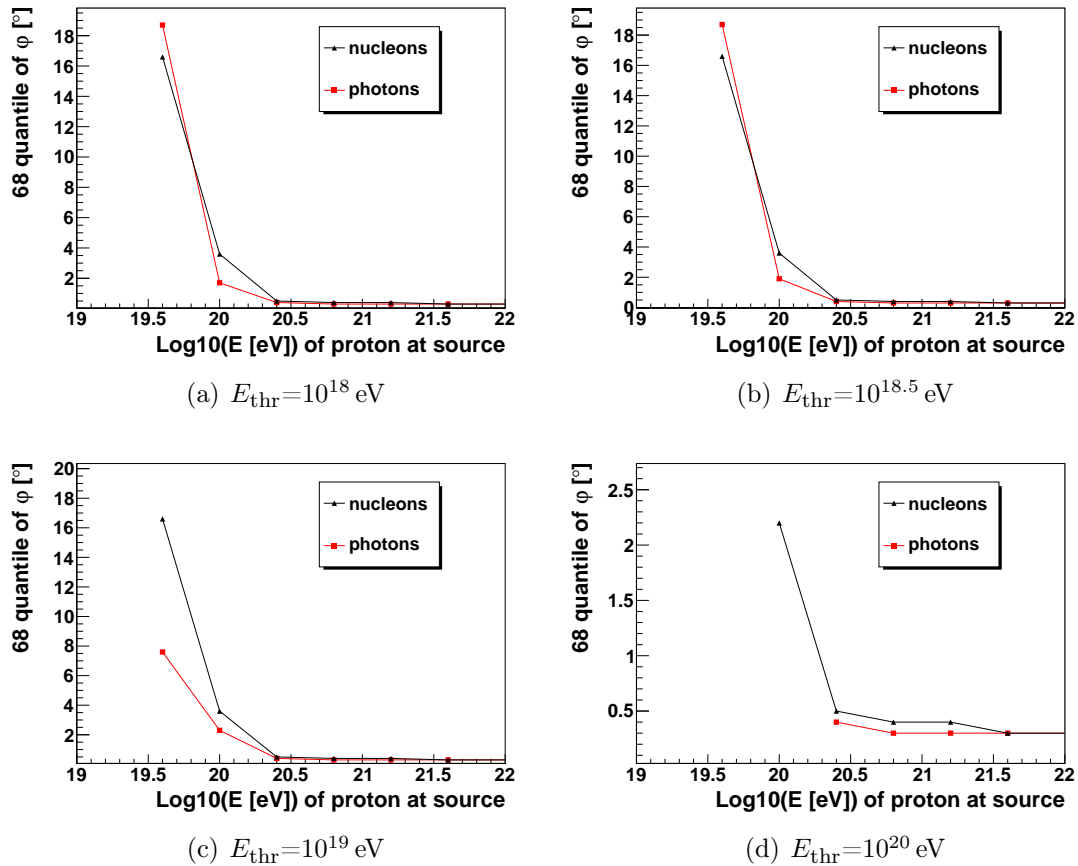
Figure 6.18: 68-quantile for the φ_{γ} (red) and the φ_{n} (black) distribution in dependence on the energy threshold of the primary protons for a source distance of $10\,\mathrm{Mpc}$ and the Miniati magnetic field, for different energy thresholds of $10^{18.5}\,\mathrm{eV}$, $10^{18.5}\,\mathrm{eV}$, $10^{19}\,\mathrm{eV}$ and $10^{20}\,\mathrm{eV}$
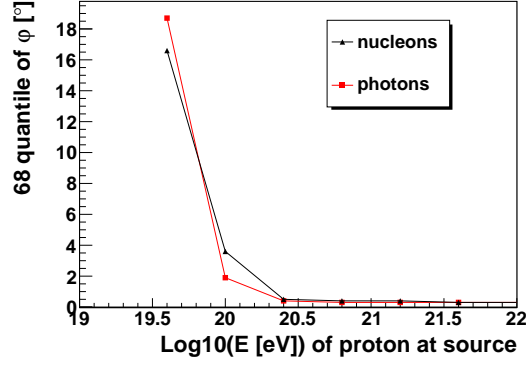
(a) Structured magnetic field by Miniati et al.[16]
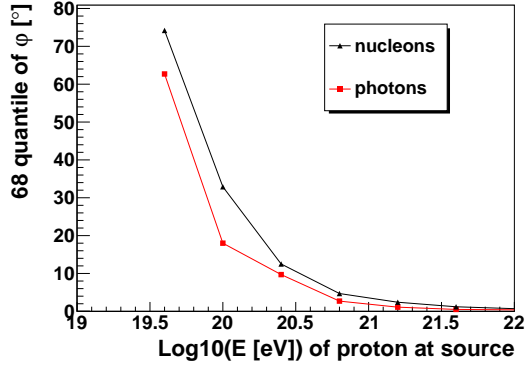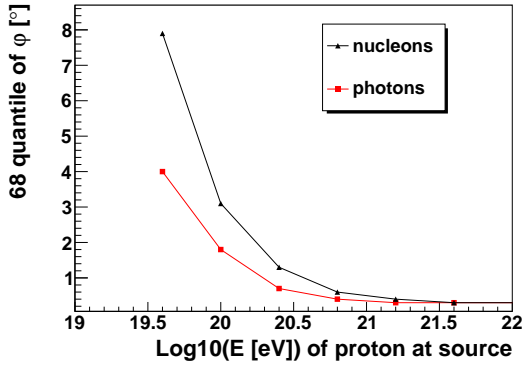
(b) Homogeneous magnetic field with B=1 nG

(c) Homogeneous magnetic field with B=10 nG

Figure 6.19: 68-quantile for the φ_γ (red) and the φ_n (black) distribution in dependence on the energy threshold of the primary protons for a source distance of 10 Mpc for three different magnetic field scenarios

(a) $E_{\text{thr}}=10^{18}$ eV

(b) $E_{\text{thr}}=10^{18}$ eV

(c) $E_{\text{thr}}=10^{19}$ eV

(d) $E_{\text{thr}}=10^{19}$ eV

(e) $E_{\text{thr}}=10^{20}$ eV

(f) $E_{\text{thr}}=10^{20}$ eV
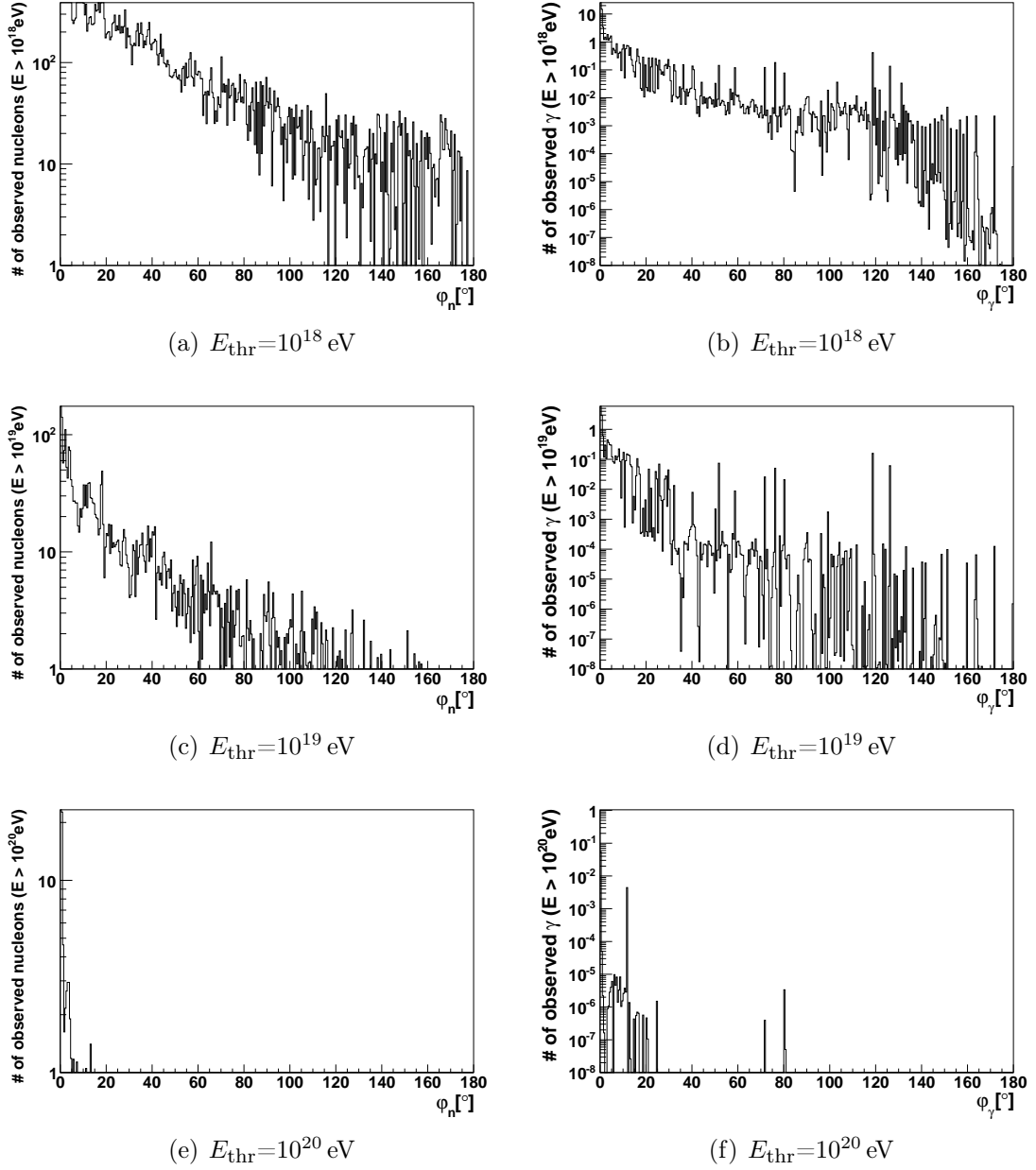
Figure 6.20: φ_{n} (left)and φ_{γ} (right) distribution assuming the Minati magnetic field and an E^{-2}-spectrum at source. Energy thresholds are 10^{18} eV, 10^{19} eV and 10^{20} eV and cutoff energy of $10^{20.5}$ eV is assumed

6.4.3 Energy spectrum of E^{-2}

In the end again the φ_γ and φ_n distribution for a complete energy spectrum from 10^{18} eV to 10^{22} eV which follows an E^{-2} power law is regarded, using the same reweighting procedure like in the previous section. The resulting φ_γ and φ_n distributions are shown in figure 6.20 for different threshold energies for the observed particles. The 68-quantile values for the two distributions in dependence on this threshold is displayed in figure 6.21(a) for a cutoff energy of the spectrum of $10^{20.5}$ eV. For this source distance of 10 Mpc one can see nearly no difference of the arrival directions of 68-quantile of the photons above 10^{18} eV from the source direction. For the nucleons, a 68-quantile value below 1° is reached above an energy threshold of 10^{20} eV. Raising the cutoff energy of the spectrum leads to a complete agreement of the 68-quantile of the φ_γ distribution with the source direction for all energy threshold at the observer as shown in figure 6.21(b).

(a) $E_{\mathrm{cut}}=10^{20.5}$ eV

(b) $E_{\mathrm{cut}}=10^{22}$ eV
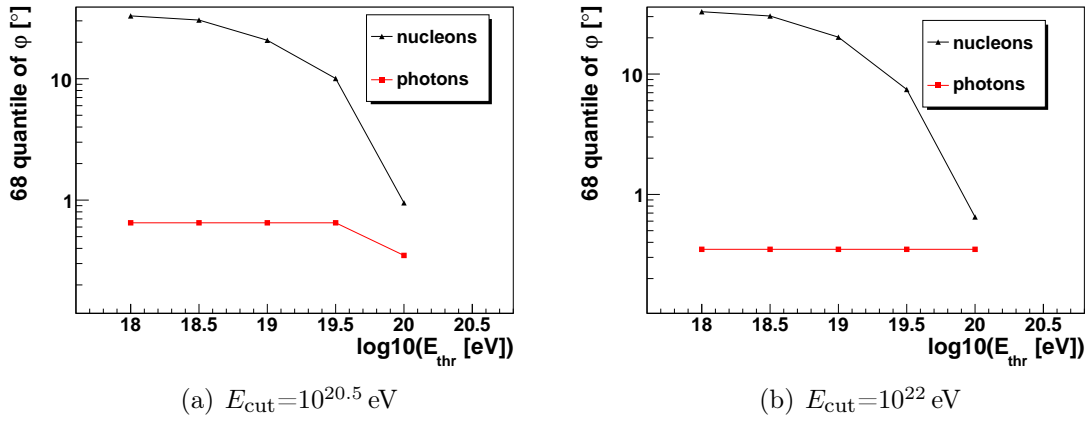
Figure 6.21: 68-quantile for the φ_γ (red) and the φ_n (black) distribution in dependence on different energy thresholds, assuming the Miniati magnetic field and an E^{-2}-spectrum at source, for cutoff energies of $10^{20.5}$ eV and 10^{22} eV

7 Conclusion and Outlook

The first part of this thesis had the aim to study the amount of photons expected from the propagation of UHE nucleons with different discrete energies at source and different source distances. The main results are shown in the matrices in figure 5.4 in chapter 5.3. These matrices show the existent of a distance for the sources of UHE protons that provides a maximum number of photons above a given detection threshold for every source energy. A parameterisation is found for this special distance and the corresponding amount of photons in depending on the starting energy of the source protons.

With the data contained in each of this matrices one could in a next step calculate the expected photon to proton ratio above different detecting thresholds for sources that emit protons with a powerlaw energy spectrum. The results could then be compared with current upper limits set by experiments like the Pierre Auger Observatory as described in section 2.4.

In the second part it was examined, how the distribution of the arrival directions of nucleons emitted from a point source behave in comparison to the distribution of the arrival directions of the photons that are produced during the propagation of this nucleons in the presents of magnetic fields. This is done in dependence on the energy of the nucleons at the source and for a complete source spectrum. Both cases are done for different photon energy ranges and magnetic field assumptions. In all cases the photons point back closer to the source of the nucleon, than the nucleon itself. The current search for sources of UHE cosmic rays by the Pierre Auger Observatory shows that cosmic rays at the highest energies do not have isotropic arrival directions [8]. The detection of UHE photons should improve the significance of this efforts and could even lead to the discovery of the sources of cosmic rays.

To increase the significance of the results in this second part, a consideration of the uncertainties should be added. The next steps would be to consider intergalactic magnetic fields, that reflect the magnetic structure in our Universe as described for example in [29] and [30]. These fields would allow predictions for different assumptions of sources distributions of UHECR. For a further improvement of the deflection studies one could consider to integrate galactic magnetic fields in the simulation. Additionally, these studies should be redone with sources that emit higher nuclei.

Acknowledgement

A Studies with a three dimensional propagation model

(a) D=3.9 Mpc
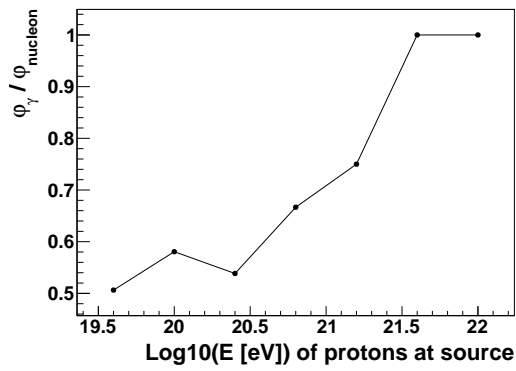
(b) D=10 Mpc
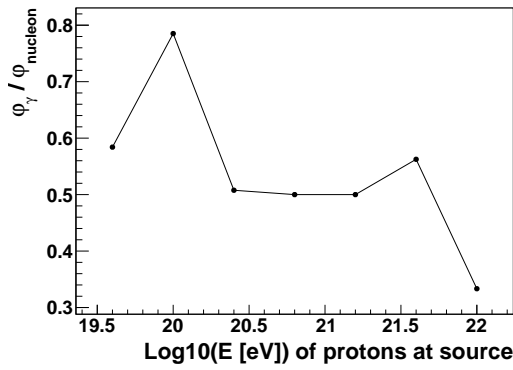
(c) D=40 Mpc
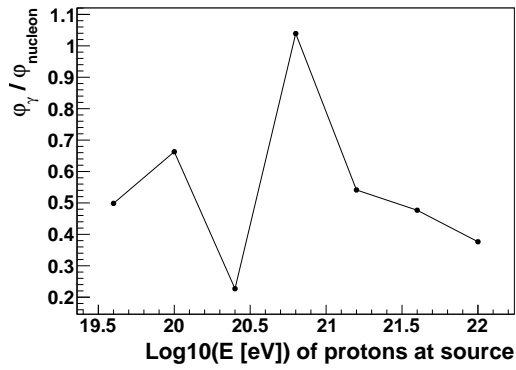
(d) D=75 Mpc

Figure A.1: ratio of the 68-quantile values for the φ_γ and the φ_n distribution in dependence on the energy of the primary protons for the source distances of 3.9 Mpc, 10 Mpc, 40 Mpc and 75 Mpc and a homogeneous magnetic field of 1 nG

(a) D=3.9 Mpc

(b) D=10 Mpc

(c) D=40 Mpc
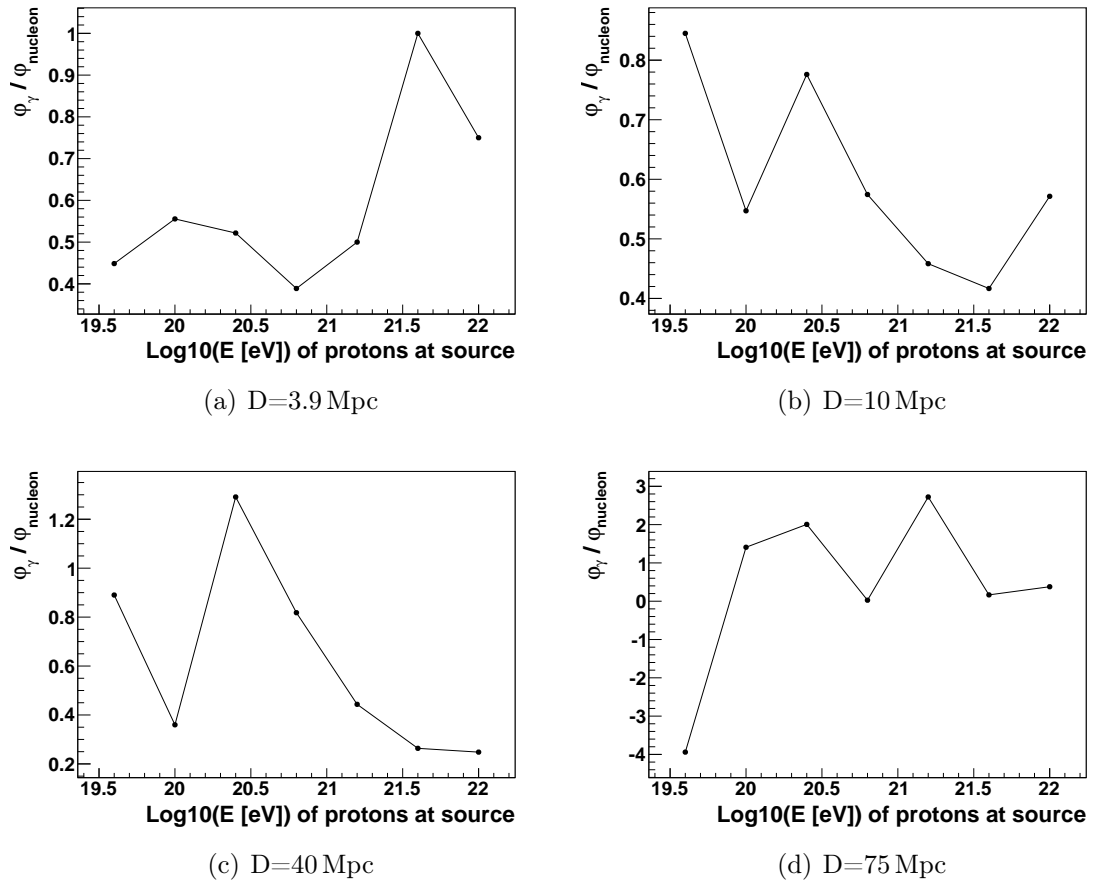
(d) D=75 Mpc

Figure A.2: ratio of the 68-quantile values for the φ_γ and the φ_n distribution in dependence on the energy of the primary protons for the source distances of 3.9 Mpc, 10 Mpc, 40 Mpc and 75 Mpc and a homogeneous magnetic field of 10 nG

(a) D=3.9 Mpc, $E_{\text{thr}}=10^{18.5}$ eV (b) D=3.9 Mpc, $E_{\text{thr}}=10^{19}$ eV (c) D=3.9 Mpc, $E_{\text{thr}}=10^{20}$ eV

(d) D=10 Mpc, $E_{\text{thr}}=10^{18.5}$ eV (e) D=10 Mpc, $E_{\text{thr}}=10^{19}$ eV (f) D=10 Mpc, $E_{\text{thr}}=10^{20}$ eV

(g) D=40 Mpc, $E_{\text{thr}}=10^{18.5}$ eV (h) D=40 Mpc, $E_{\text{thr}}=10^{19}$ eV (i) D=40 Mpc, $E_{\text{thr}}=10^{20}$ eV

(j) D=75 Mpc, $E_{\text{thr}}=10^{18.5}$ eV (k) D=75 Mpc, $E_{\text{thr}}=10^{19}$ eV (l) D=75 Mpc, $E_{\text{thr}}=10^{20}$ eV
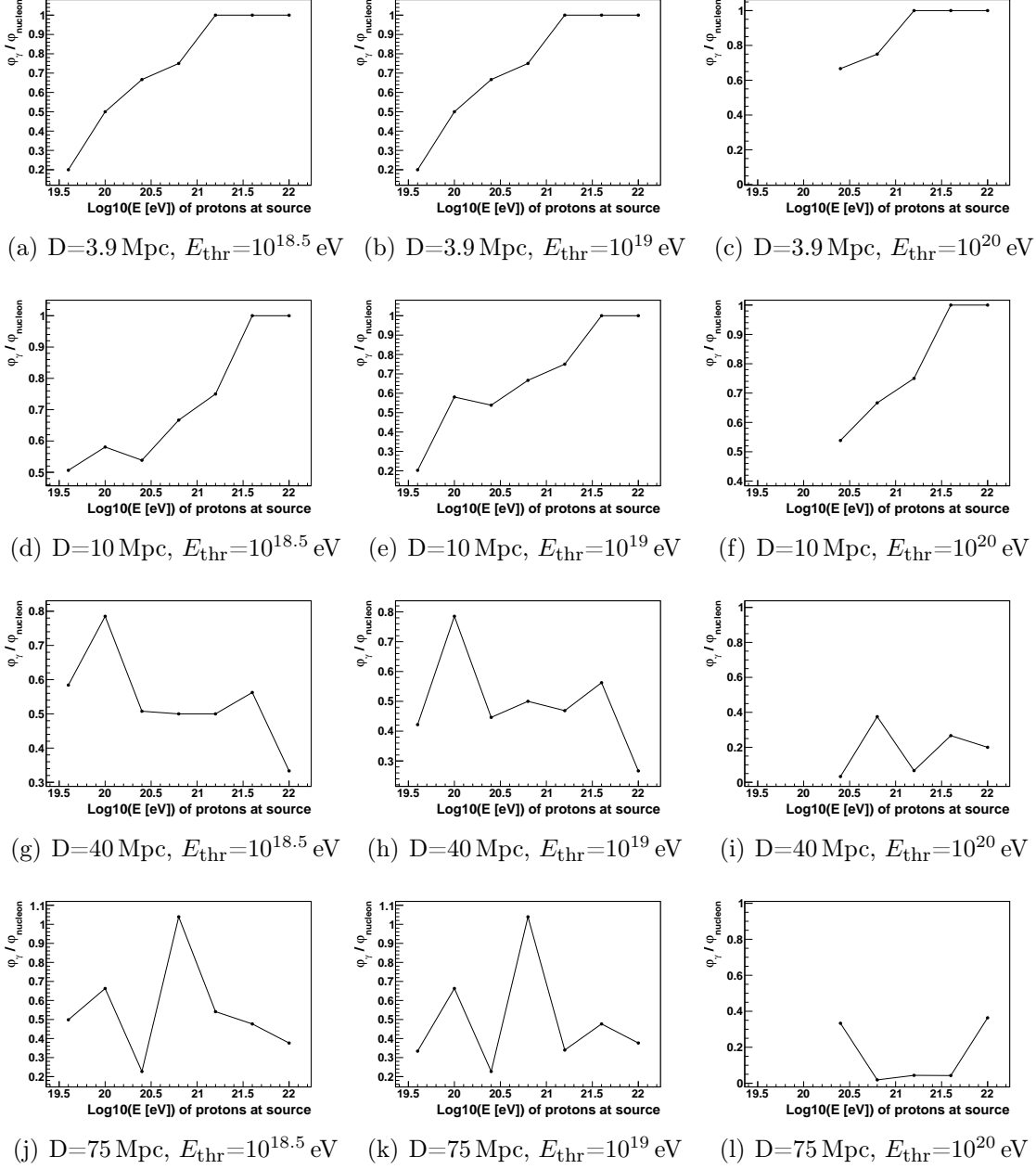
Figure A.3: ratio of 68-quantile for the φ_γ and the φ_n distribution in dependence on the energy of the primary protons for different source distances (colums) and for the different energy thresholds (rows) for a homogeneous magnetic field of 1 nG

Bibliography

[1] E. Armengaud, G. Sigl, T. Beau, and F. Miniati, "CRPropa: A numerical tool for the propagation of UHE cosmic rays, gamma-rays and neutrinos," *Astropart. Phys.* **28** (2007) 463–471, arXiv:astro-ph/0603675.

[2] J. W. Cronin, S. P. Swordy, and T. K. Gaisser, "Cosmic rays at the energy frontier," *Sci. Am.* **276** (1997) 32–37.

[3] J. Bluemer, R. Engel, and J. R. Hoerandel, "Cosmic Rays from the Knee to the Highest Energies," *Prog. Part. Nucl. Phys.* **63** (2009) 293–338, arXiv:0904.0725 [astro-ph.HE].

[4] K. Greisen, "End to the cosmic ray spectrum?," *Phys. Rev. Lett.* **16** (1966) 748–750.

[5] G. Zatsepin and V. Kuzmin, "Upper limit of the spectrum of cosmic rays," *JETP Lett.* **4** (1966) 78–80.

[6] **HiRes Collaboration**, R. Abbasi *et al.*, "Observation of the GZK cutoff by the HiRes experiment," *Phys. Rev. Lett.* **100** (2008) 101101, arXiv:astro-ph/0703099.

[7] **Pierre Auger Collaboration**, J. Abraham *et al.*, "Observation of the suppression of the flux of cosmic rays above 4×10^{19}eV," *Phys. Rev. Lett.* **101** (2008) 061101, arXiv:0806.4302 [astro-ph].

[8] **Pierre Auger Collaboration**, J. Abraham *et al.*, "Correlation of the highest energy cosmic rays with nearby extragalactic objects," *Science* **318** (2007) 938–943, arXiv:0711.2256 [astro-ph].

[9] M. Risse and P. Homola, "Search for ultra-high energy photons using air showers," *Mod. Phys. Lett.* **A22** (2007) 749–766, arXiv:astro-ph/0702632.

[10] **The Pierre Auger Collaboration**, J. Abraham *et al.*, "Upper limit on the cosmic-ray photon fraction at EeV energies from the Pierre Auger Observatory," *Astropart. Phys.* **31** (2009) 399–406, arXiv:0903.1127 [astro-ph.HE].

[11] **Pierre Auger Collaboration**, J. Abraham *et al.*, "Upper limit on the cosmic-ray photon flux above 10^{19} eV using the surface detector of the Pierre Auger Observatory," *Astropart. Phys.* **29** (2008) 243–256, `arXiv:0712.1147 [astro-ph]`.

[12] R. Beck, "Magnetic fields in nearby galaxies: prospects with future radio telescopes," `arXiv:0909.0162 [astro-ph.CO]`.

[13] T. E. Clarke, "Faraday Rotation Observations of Magnetic Fields in galaxy Clusters," *J. Korean Astron. Soc.* **37** (2004) 337–342, `arXiv:astro-ph/0412268`.

[14] Y. Xu, P. P. Kronberg, S. Habib, and Q. W. Dufton, "A Faraday Rotation Search for Magnetic Fields in Large Scale Structure," *Astrophys. J.* **637** (2006) 19–26, `arXiv:astro-ph/0509826`.

[15] L. Biermann *Z. Naturf.* **A5** (1950) 65.

[16] F. Miniati, "Inter-galactic Shock Acceleration and the Cosmic Gamma-ray Background," *Mon. Not. Roy. Astron. Soc.* **337** (2002) 199, `arXiv:astro-ph/0203014`.

[17] G. Sigl, F. Miniati, and T. A. Ensslin, "Ultra-high energy cosmic ray probes of large scale structure and magnetic fields," *Phys. Rev.* **D70** (2004) 043007, `arXiv:astro-ph/0401084`.

[18] S. Lee, "On the propagation of extragalactic high-energy cosmic and gamma-rays," *Phys. Rev.* **D58** (1998) 043004, `arXiv:astro-ph/9604098`.

[19] J. R. Primack, J. S. Bullock, and R. S. Somerville, "Observational gamma-ray cosmology," *AIP Conf. Proc.* **745** (2005) 23–33, `arXiv:astro-ph/0502177`.

[20] E. Armengaud and T. Beau, "The CRPropa framework: A numerical tool to study propagation effects on UHECRs and their secondaries in the Local Universe,".

[21] A. Franceschini, H. Aussel, C. Cesarsky, D. Elbaz, and D. Fadda *Astron. Astrophys.* **378** (2001) .

[22] R. J. Protheroe and P. L. Biermann, "A new estimate of the extragalactic radio background and implications for ultra-high-energy gamma ray propagation," *Astropart. Phys.* **6** (1996) 45–54, `arXiv:astro-ph/9605119`.

[23] T. A. Clark, L. W. Brown, J. K. Alexander, D. Elbaz, and D. Fadda *Nature* **228** (1970) 847.

[24] G. Cowen, *Statistical Data Analysis*. Oxford University Press, 1998.

[25] D. De Marco, P. Blasi, and A. V. Olinto, "On the statistical significance of the GZK feature in the spectrum of ultra high energy cosmic rays," *Astropart. Phys.* **20** (2003) 53–65, `arXiv:astro-ph/0301497`.

[26] C. Grupen, *Astroteilchenphysik*. Vieweg Verlag, 2000.

[27] **Pierre Auger Collaboration**, M. Ave, "Reconstruction accuracy of the surface detector array of the Pierre Auger Observatory," `arXiv:0709.2125 [astro-ph]`.

[28] G. Sigl, "private communication,".

[29] K. Dolag, D. Grasso, V. Springel, and I. Tkachev, "Constrained simulations of the magnetic field in the local universe and the propagation of UHECRs," *JCAP* **0501** (2005) 009, `arXiv:astro-ph/0410419`.

[30] J. Donnert, K. Dolag, H. Lesch, and E. Muller, "Cluster Magnetic Fields from Galactic Outflows," `arXiv:0808.0919 [astro-ph]`.

Hiermit versichere ich, dass ich diese Arbeit nur unter Zuhilfenahme der angegebenen Quellen und Hilfsmittel selbstständig angefertigt habe.

Wuppertal, 30.07.2010   Biswajit Sarkar

66